BIOMEDICAL ENGINEERING MSc PROGRAM
UNIVERSITY OF CRETE
TECHNICAL UNIVERSITY OF CRETE
FOUNDATION FOR RESEARCH AND TECHNOLOGY-HELLAS

Application Grade Thesis

Quantifying cell-matrix interactions in laser microfabricated scaffolds

Moschogiannaki Fereniki

Supervisor's Name: Dr. Emmanuel Stratakis

2nd member committee name: Prof. Dimitrios Tzeranis

3rd member committee name: Prof. Ioannis Charalampopoulos

Date of completion: 30/06/2022

This dissertation is submitted as a partial fulfilment of the requirements for the Master's degree of Biomedical Engineering M.Sc. program

Acknowledgements

I would like to thank my supervisor Dr. Emmanuel Stratakis who gave me again the opportunity to work in his laboratory and be part of his great team. I also want to thank my supervisor Prof. Dimitrios Tzeranis for his guidance and his inspiration. Also, I would like to thank the lab team for their help and their support, especially Constantina Georgelou. Finally, I want to thank my family, my friends and Dimitri.

Abstract

This thesis studies how cell phenotypes of interest can be regulated by the physicochemical properties of their surrounding insoluble microenvironment (matrix). Specifically, it studies how the microfabrication of specific μm-sized patterns in porous collagen-based scaffolds (PCS) can regulate key phenotypes of fibroblasts and Neural Stem Cells, two cell types involved in wound healing. By using Fs laser ablation, three different patterns were microfabricated on the scaffolds. In addition to the ''plain'' control PCS, ablation enabled the fabrication of a PCS with parallel horizontal lines, a PCS with concentric circles and a PCS that contained a hole in its center. The first experiment monitored the contractile response of fibroblasts when seeded in PCS that contained various microfabricated patterns. Live cell imaging revealed significant PCS deformation due to fibroblast contraction. Immunolabeling for α smooth muscle actin (α-SMA) in the PCS that contained concentric cycles revealed the presence of α-SMA$^+$ cells (myofibroblasts) on the outer surface of circular features. The second experiment studied whether differentiation of Neural Stem Cells towards neurons and astrocytes depend on the presence and type of microfabricated features. Immunolabeling for Tuj1 (neurons) and GFAP (astrocytes) revealed that PCS with concentric circles decreased the fraction of cells that differentiated towards neurons and astrocytes. This thesis provides a first proof of concept that microfabricated features in PCS can regulate cell phenotypes, although it did not study in detail its underlying molecular mechanisms.

Table of contents

List of figures

List of tables

Chapter 1: Introduction

This thesis studies how the properties of a 3D matrix regulate cell function. More specifically, this thesis probes how the structure of porous collagen-based scaffolds (PCS), a particular class of biomaterial, regulate two different types of mouse cells (fibroblasts, embryonic neural stem cells). It focuses on quantifying cell-matrix interactions when cells are seeded in laser microfabricated scaffolds. Fs laser ablation is utilized to microfabricate specific structures on the scaffold, thereby altering scaffold structure and modifying the mechanical properties (stiffness) sensed by seeded cells. By seeding cells inside scaffolds microfabricated in particular ways, this study probes whether such microstructures can regulate key cell phenotypes (proliferation, differentiation) of interest.

It is well known that the mechanical properties of biomaterials or tissues regulate the cells in physiology and pathology. The development of means for quantifying cell-matrix interactions can provide better understand on tissue physiology and disease pathology. Such knowledge can also be utilized to design better biomaterials for tissue regeneration e.g. wound healing and injury restoration. Along this direction, literature suggests that biomaterial properties (porosity, pore size, pore shape and material stiffness) relate to the mechanical microenvironment sensed by cells, thereby strongly affect the ability of a biomaterial graft to induce tissue regeneration by affecting cell commitment, migration, proliferation and early matrix formation.

First in Chapter 2: State-of-the-art, a quantification of cell traction forces on flat and 3D substrates will be given. Also, according to bibliography the regulation of cell phenotypes by scaffold properties will be mentioned. In Chapter 3 the experimental methods will be described. Furthermore, in Chapter 4 the results are shown in two categories: ‘’NIH-3T3 growth in PCS’’ and ‘’NCSs growth in PCS’’. Lastly, the Chapter 5: Discussion and analysis of findings is followed.

Chapter 2: State-of-the-art

Cells seeded inside a biomaterial bind to their surrounding matrix and exert forces that deform the matrix. Cells' behavior inside a biomaterial depends on the microenvironment that cells perceive, including its chemical composition, topology, and mechanical properties. In particular, the mechanical environment perceived by a cell can be described via an equivalent matrix stiffness, described by a spring of spring constant k and length L. In this case, the force F applied by a cell and the resulting matrix deformation δL is related by Hooke's law

$$k=F/\delta L$$

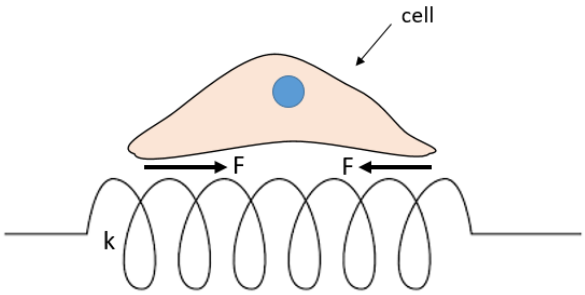

Figure 1: Schematic representation of cell perception of matrix stiffness. When a cell binds and exerts a pair of forces F to the matrix, the matrix is deformed *by a distance δL. The spring constant k represents the* matrix's *stiffness k, defined as the ratio F/δ*L.

This thesis focuses how the mechanical properties of the matrix regulate key phenotypes of seeded cells. Quantification of cell phenotypes is relatively straightforward by existing methods of proteomics, genomics and imaging. On the other hand, quantification of the equivalent matrix stiffness k is much more challenging, as it requires means to measure the force F applied by cells and the resulting deformation δL of the matrix. The following two sections summarize published means for studying cell-matrix mechanical interactions on flat substrates or inside 3D biomaterials.

2.1 Quantifying Cell Traction Forces on Flat Substrates

Stabley et al. describe a method for measuring the force transmitted when the epidermal growth factor receptor (EGFR) binds to its ligand EGF [1]. They used a fluorescence-based sensor to map the mechanical strain exerted by specific cell-surface proteins in living cells. Such a sensor can spatially and temporally map those forces. In one terminus of the sensor there is a flexible linker covalently conjugated to a biological ligand. The sensor is anchored onto a surface so that forces not to translocate the sensor. The linker is made of polyethylene glycol (PEG) polymer, due to its biocompatibility and minimal interactions with other biomolecules. When cellular forces are exerted on the ligand, the linker extends from its relaxed state and the fluorophore is moved away from the quencher. This results in increased fluorescence intensity that maps mechanical tension and can be detected by conventional fluorescence microscopes.

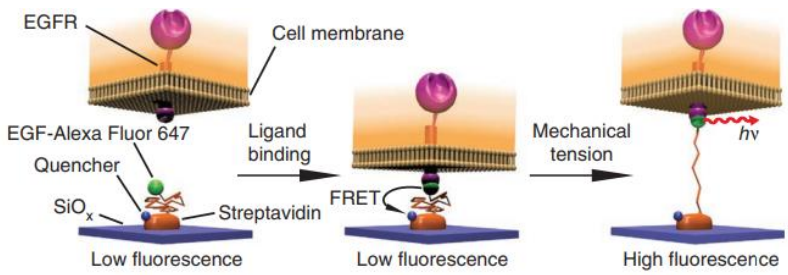

Figure 2: Schematic of fluorescence force sensor function. When EGFR exerts a force on its ligand, the flexible PEG linker extends. Displacement of the EGF ligand away from the quencher results in increased fluorescence intensity, thus reporting the transmission of mechanical tension through the EGF-EGFR complex[1].

Dembo et al. describe a method for quantifying traction forces exerted by 3T3 fibroblasts during locomotion[2]. They observed that fibroblast lamellipodia can generate intense traction stress. They deposited a ~70 μm thick polyacrylamide layer on a glass coverslip. In order to visualize polyacrylamide deformations, they embedded randomly in the polyacrylamide fluorescent latex beads of 0.2 μm diameter. As cells adhere, spread, and locomote on the substrate they apply traction stresses that displace beads. A digital image of the field was recorded. Upon trypsin treatment (disrupted adhesive contacts) beads recoiled to their undisturbed positions. By taking a second image the displacement of each bead was computed. Their method estimated that the magnitude of stress applied over the entire projected area under a cell is 20 kdyn/cm^2 (2000 pN/m^2).

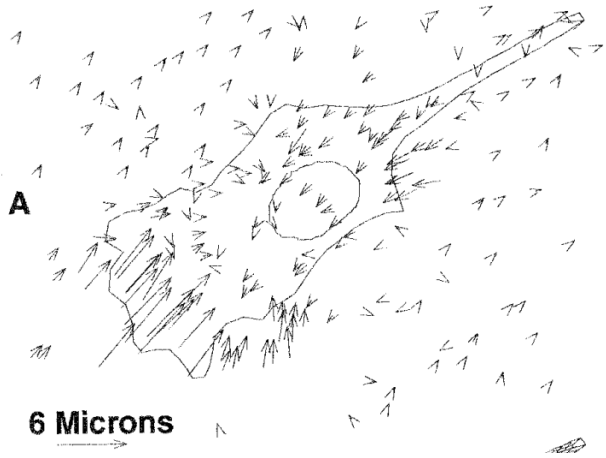

Figure 3: Map of displacement vectors (three times actual size) of marker beads induced by cell traction[2].

Tan et al. used microfabricated arrays of elastomeric, microneedle-like posts in order to measure the mechanical interactions between cells and their substrates[3]. The substrates called microfabricated post-array-detectors (mPADs) were fabricated by replica-molding. Posts, made of silicone elastomer, were closely spaced and were designed to encourage cells to attach and spread across them, causing post bending. For small deflections, posts behave like linear springs. The resulting beam deflection δ induced by the applied transverse force F

can be estimated based on the following equation that describes pure bending of an elastic beam:

$$F = \left(\frac{3EI}{L^3}\right)\delta$$

where E, I, L are the Young's modulus, area moment of inertia and beam length respectively. These parameters are known and can be utilized to estimate the linear spring relationship

$$F = k \cdot \delta$$

The deflection δ of each post was quantified via immunofluorescence microscopy. Based on the post deflections, cell forces were estimated to be greater than 12 nN.

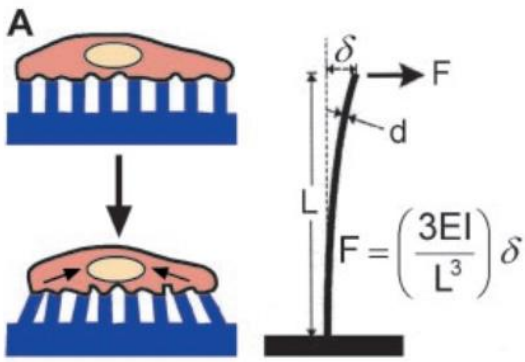

Figure 4: Quantifying cell traction forces using mPADS substrates. A cell spreads across multiple elastomeric posts and exerts traction forces that deflect posts[3]. The force F applied by the cell is estimated based on standard beam bending formulas based on the measured longitudinal deformation δ.

2.2 Quantifying Cell Traction Forces inside 3D Biomaterials

Cells exhibit different morphology, cytoskeletal organization and focal adhesion structure when they are encapsulated in a 3D matrix rather than when grown on 2D substrates[4]. Traction forces exerted by cells were measured by Legant et al. using polyethylene glycol (PEG) hydrogels of E=600–1,000 Pa Young's modulus. Hydrogels incorporated proteolytically degradable domains in their polymer backbone and pendant adhesive ligands. Matrix deformation was quantified by tracking the displacements of 60,000–80,000 fluorescent beads in the vicinity of each cell. Confocal images were used to generate a finite element mesh of the hydrogel surrounding the cell. Bead displacements were calculated by constructing a discretized Green's function, applying unit tractions to each facet on the surface of the cell mesh and solving the finite element equations. They found that cells exerted tractions of 100–5,000 Pa and that strong forces were located predominantly near the tips of long, slender extensions. Generally, tractions increased as a function of the distance away from the cell's center of mass.

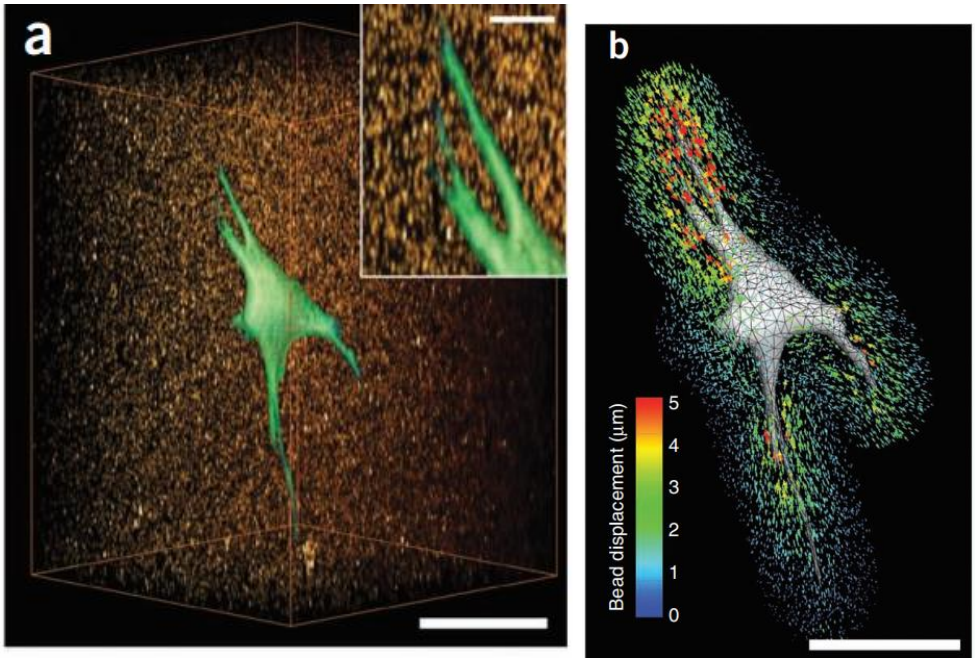

Figure 5: Visualizing cell-induced hydrogel deformations. (a) Volume rendering of an EGFP-expressing NIH-3T3 fibroblast (green) spreading inside a 3D hydrogel containing fluorescent beads (red). Scale bar, 50 µm (10 µm in inset). (b) Measured bead displacement trajectories color coded by magnitude[4]. Scale bar, 50 µm.

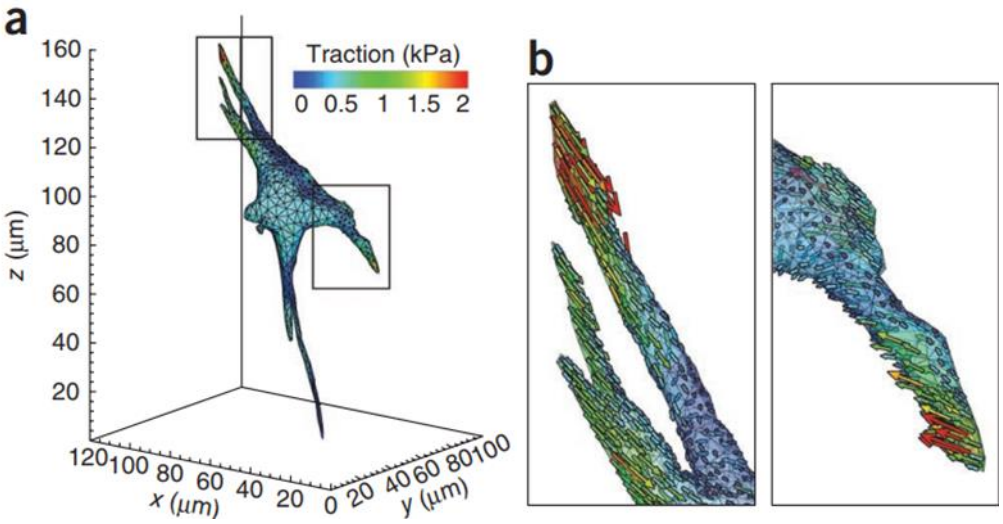

Figure 6: (a) Contour plot of traction exerted by a cell. (b) Magnification of sections outlined in a, show individual traction vectors on each facet[4].

Using computational modeling along with engineered epithelial tissues of precise geometry, Gjorevski et al. tried to define the experimental parameters in order to directly measure the mechanical stress profile of 3D epithelial tissues surrounded by a matrix of native type I collagen[5]. In order to visualize tissue-induced matrix deformations, they dispersed 1 µm diameter fluorescent polystyrene beads in the neutralized collagen solution at high density (~4×10^8 beads/ml). By collecting confocal stacks before and after relaxing the tissues and by extracting the 3D and in-plane bead displacements using the Autoregressive Motion

tracking routine in Imaris, they calculated, from the full 3D displacement field, tissue-induced strains within the collagen gel defined as

$$\varepsilon_{ij} = \frac{1}{2}\left(\frac{\partial u_i}{\partial x_j} + \frac{\partial u_j}{\partial x_i}\right)$$

where i=1, 2, 3. In this equation ε is the strain tensor; u_i is the displacement in direction i; and x_i are rectangular spatial coordinates.

They observed that sharp displacement gradients occurred when single epithelial cells were are plated on top of a collagen gel. On the other hand, when epithelial cells were fully embedded in collagen, cells induced negligible displacements.

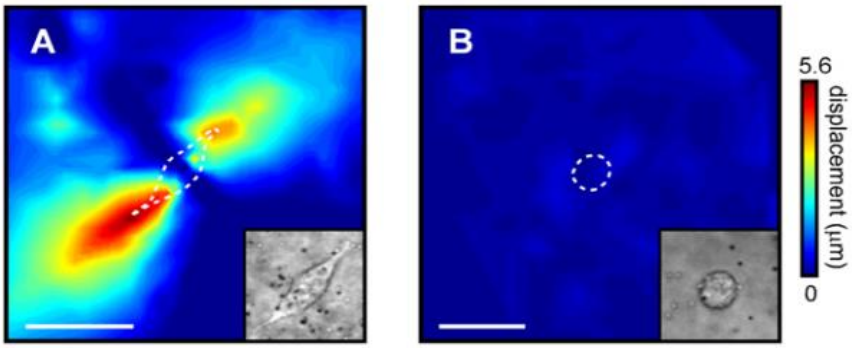

Figure 7: (A) Substrate deformation induced by a single epithelial cell plated on top of collagen gel. (B) Matrix deformation induced by a single epithelial cell fully embedded within a collagen gel[5].

Notbohm et al. developed a 3D full-field measurement technique to measure large deformations in soft materials based on a digital volume correlation (DVC) algorithm and 3D laser scanning confocal microscopy images[6]. The algorithm tracked motions of sub-volumes within 3D image datasets. They used this 3D traction force microscopy (3DTFM) technique to quantify traction forces applied by 3T3 fibroblasts on fibronectin-functionalized polyacrylamide gels. The polyacrylamide substrate is linear, elastic, and nearly incompressible, therefore the incompressible form of Hooke's Law was used to compute the stress tensor based on the strain tensor. Traction forces applied by cells to the top surface of the polyacrylamide gel are computed using the Cauchy relation.

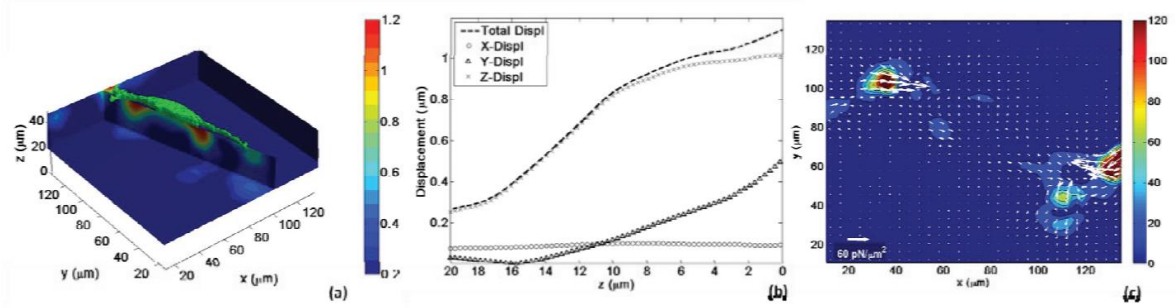

Figure 8: A migrating fibroblast deforms to the substrate beneath it (a). The displacements under the cell at the top of the substrate (b) indicate that the cell applies displacements in all directions. The traction forces applied

by the cell are shown in (c). Colors indicate the magnitude of 3D traction forces, while arrows show the direction of the traction force along the in-plane (x-y). Data show that the cell pulls inward (indicated by white arrows) with maximum magnitude of 120 pN/µm^2 [7].

2.3 Regulation of Cell Phenotypes by Scaffold Properties

Several studies have identified that cell phenotypes are regulated by their immediate insoluble microenvironment, i.e. the matrix. In agreement with this observation, once cells are seeded inside a Porous Collagen-Based Scaffold (PCS), their phenotypes are regulated by elementary interactions with the PCS, which depend on PCS physicochemical properties. This section summarizes papers that report how PCS physicochemical properties regulate phenotypes of interest in seeded cells.

Herrera et al. studied the mechanical environment perceived by human bone marrow-derived mesenchymal stromal cells (hBMSCs) when they are seeded inside highly aligned porous collagen scaffolds[8]. They developed finite element (FE) models of different scaffold prototypes in order to quantify stiffness in the microscopic and macroscopic level. Four collagen scaffold prototypes of different mass content were produced (0.8%, 1.1%, 1.5% and 3.0% wt/wt%). 3D imaging and image processing was utilized to quantify several structural features of the scaffolds. Results (Figure 9) revealed that several structural properties (thickness T of scaffold walls, strut density N) depended on the mass content, while other did not (scaffold wall distance W) or depended slightly (period and amplitude of wall wave-like pattern).

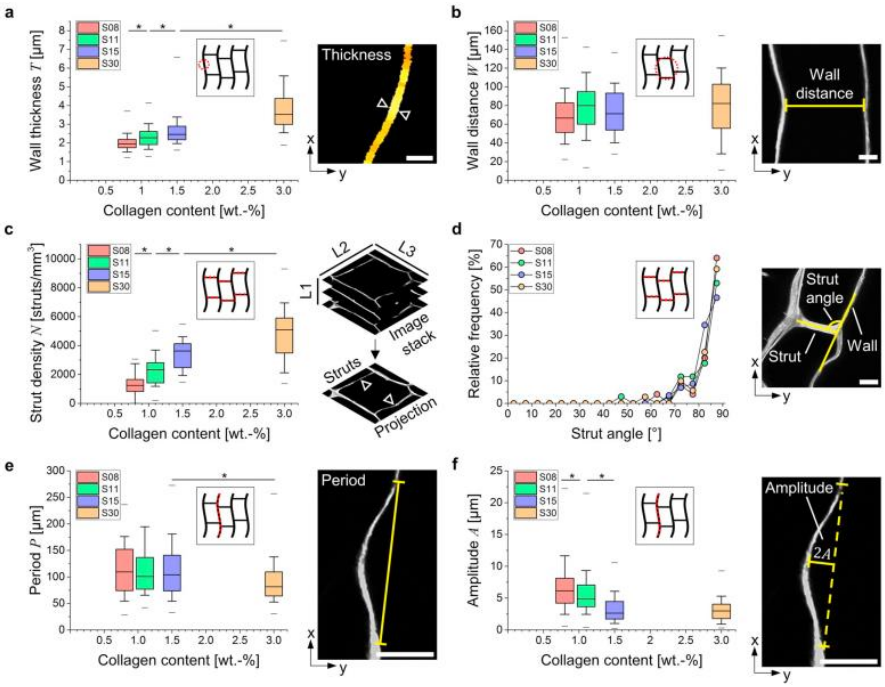

Figure 9: Key structural parameters of highly aligned macroporous collagen scaffolds depend on their mass density[8].

The same study also quantified the stiffness of the same four scaffold prototypes in three levels. First, the macroscopic scaffold stiffness $S_{SCAFF\text{-}EXP}$ was quantified experimentally via monoaxial mechanical compression tests. Results show that $S_{SCAFF\text{-}EXP}$ increased strongly with increasing scaffold mass content. Second, AFM measurements showed that the elastic moduli of the scaffold walls $E_{WALLEXP}$ increased with scaffold mass content.

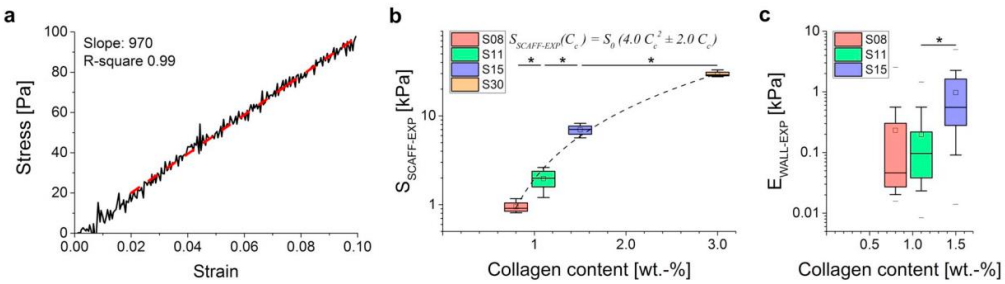

Figure 10: Stiffness of the four scaffold prototypes as a function of their mass density[8].

Finally, the cell-effective stiffness S_{EFF} (a metric of the stiffness sensed by an individual adherent cell) was estimated using FE modeling. Simulation results show that S_{EFF} increased with increasing collagen mass content. The empirical relationship $S_{EFF}/S_{SCAFF} = 6.4 \pm 0.6$ was proposed, indicating that the stiffness perceived by cells is approximately 6 times larger than the macroscopic stiffness of the scaffold, yet lower than the Young Modulus of the bulk scaffold material (Figure 11).

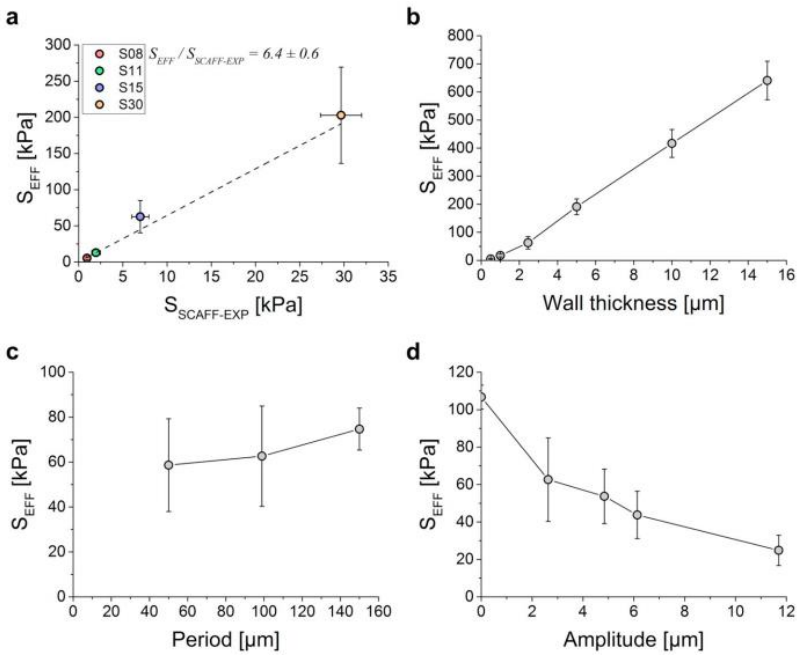

Figure 11: Relationship between measured scaffold structural parameters and numerically-estimated stiffness metrics (cell-effective stiffness S_{EFF}, macroscopic stiffness $S_{SCAFF\text{-}EXP}$) in four scaffold prototypes of increasing mass fraction[8].

HBMSCs were seeded in the four scaffold prototypes of increasing mass content in order to examine the influence of S_{EFF} on their differentiation. As shown in Figure 12, scaffold

prototypes S_{11} and S_{15} (S_{EFF} = 10.8 ± 1.5 kPa and 51.6 ± 4.3 kPa respectively) provided a pro-osteogenic, while S_{08} (S_{EFF} = 4.6 ± 0.8 kPa) provided a rather pro-adipogenic environment.

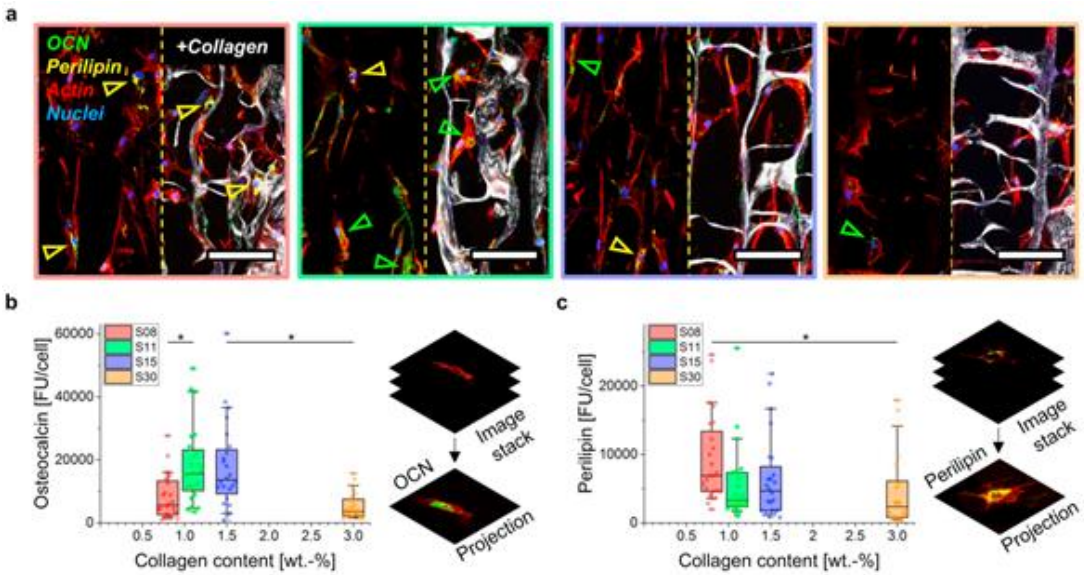

Figure 12: The effect of scaffold collagen content on the differentiation of seeded hBMSCs. HBMSCs were seeded in four scaffold prototypes of increasing collagen content and were cultured under mixed adipogenic/osteogenic medium. (a) Representative images of cells inside the four scaffold prototypes. Each image is divided in two halves delimited by the yellow dashed line. The left half depicts osteocalcin (OCN, green), perilipin (yellow), actin filaments (red) and nuclei (blue). The right half is overlaid with the collagen scaffold structure (SHG-signal). Exemplary cells positive for osteocalcin and perilipin are indicated by green and yellow arrows respectively. (b) Quantification of osteocalcin signal intensity per cell. (c) Quantification of perilipin signal intensity per cell[8].

Corin et al. examined the contractile response of normal human dermal fibroblasts (NHDFs) inside collagen-GAG scaffolds of different pore sizes when cells are seeded in different densities[9]. NHDFs are similar to cells that participate in skin wound healing. Experiments indicated that NHDFs are more contractile than the mouse 3T3 cell line. NHDFs were seeded in four different kinds of porous collagen scaffolds of same mass fraction, yet different mean pore diameter (96, 110, 121 and 151 μm). Results show that the total force exerted by all cells varies with the pore size but not with the cell density (Figure 13). The buckling force per cell F_{cell} (in nN) was correlated to the mean pore diameter d of the scaffold (in μm) and to the number of cells/pore (N_{pore}):

$$F_{cell} = \frac{1.64 \times 10^{-5} d^3}{N_{pore}}$$

The buckling force per cell F_{cell} was also expressed as a function of the cell number N_{matrix} seeded per scaffold:

$$F_{cell} = 8.86 \times 10^5 (N_{matrix})^{-1}$$

The total force in the matrix does not vary with the pore size or cell density.

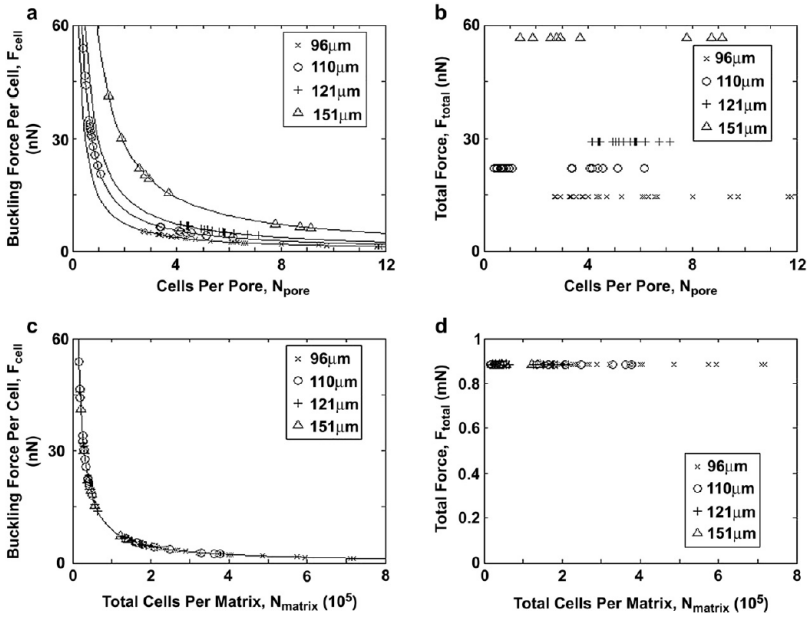

Figure 13: The force per cell and the total force plotted as a function of the number of cells attached per pore and the number of cells per matrix, for four different scaffold pore sizes at the point the scaffolds buckle[9].

Another study focused on the migratory behavior of NR6 mouse fibroblasts in collagen-glycosaminoglycan (CG) scaffolds[10]. Specifically, it investigated how the pore size and the scaffold strut elastic moduli E_s affect fibroblast migration. The study utilized CG scaffolds that had same mass fraction, yet different mean pore size (96, 110, 121, and 151 μm), achieved by using different final freezing temperatures of -10, -20, -30, and -40°C during scaffold lyophilization. Results showed that fibroblast migration in scaffolds of larger pores exhibited less dispersion and less motility than fibroblasts migrating in scaffolds of smaller pores. Further quantification, showed that cell migration speed and the motile fraction decreased significantly with increasing scaffold pore size. The pore size (in the range 96–151 μm) of the CG scaffold did not affect its modulus, as reported previously in Harley et al.[11]

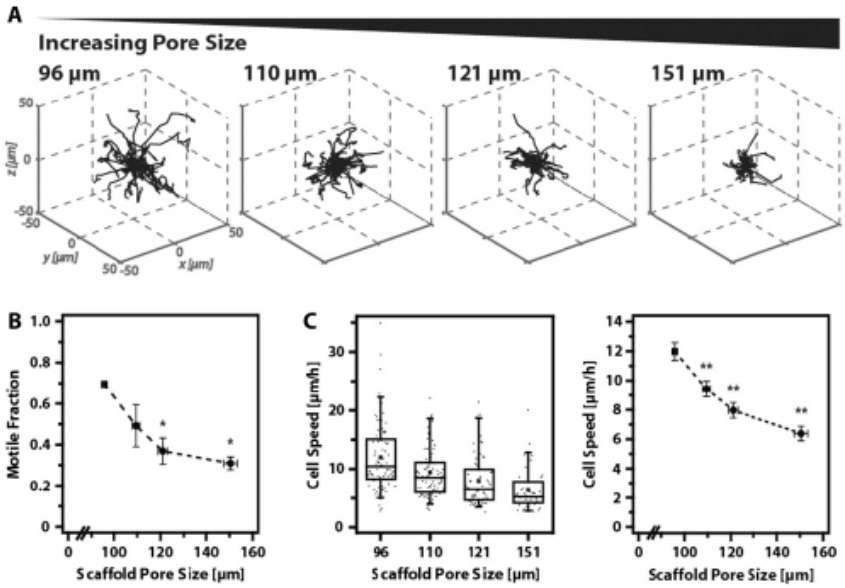

Figure 14: Cell migration behavior decreases with increasing mean scaffold pore size. Tracks of NR6 cells migrating in CG scaffolds with four distinct mean scaffold pore sizes (96–151 µm) were determined using 3D time-lapse confocal microscopy[10].

In order to vary the scaffold strut modulus E_s independently of pore size, the same study further cross-linked scaffolds of a constant pore size (96 µm) with varying ratios of 1-ethyl-3-(3-dimethylaminopropyl)carbodiimide (EDAC) to N-hydroxysuccinimide (NHS) to collagen carboxylic acid groups (COOH). Scaffolds were cross-linked via four treatments: DHT 105ºC for 24 h, 1:1:5 EDAC/NHS/COOH ratio, 5:2:5 EDAC/NHS/COOH ratio, and 5:2:1 EDAC/NHS/COOH ratio as shown in Table 1. Results showed that DHT and EDAC crosslinking did not induce microstructural (pore size) changes in CG scaffolds. Compression tests on scaffolds were performed using a custom mechanical testing device. The bending stiffness of individual struts E_s was measured by atomic force microscopy (AFM). The migration speed exhibited a biphasic behavior with strut modulus, shown in Figure 15.

Table 1: Scaffold and strut elastic moduli, motile fraction, and cell speed in cross-linked scaffold variants of NR6 fibroblasts[11].

Cross-linking treatment	Scaffold elastic moduli (E^*) (Pa)	Scaffold strut elastic moduli (E_s) (MPa)	Motile fraction	Cell speed (μm/h)
DHT (standard)	206 ± 36	5.28 ± 0.25	0.69	10.84 ± 0.54
EDAC1:1:5	225 ± 11	10.6 ± 0.50*	0.75	12.53 ± 0.42*
EDAC5:2:5	410 ± 30*	11.8 ± 0.56**	0.86	15.35 ± 0.56**
EDAC5:2:1	1480 ± 210**	38.0 ± 1.8***	0.77	12.25 ± 0.64*

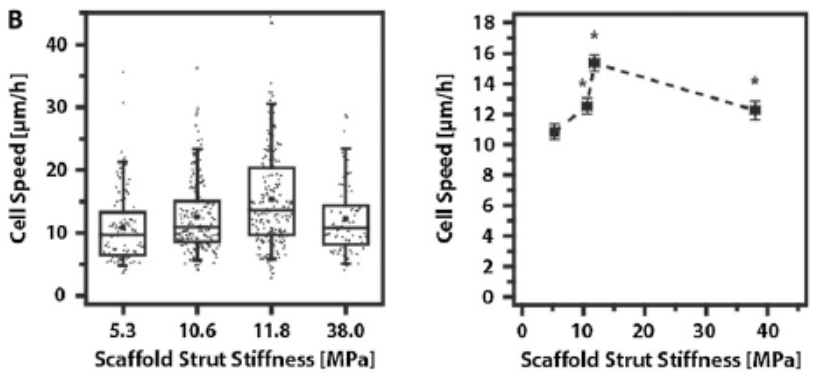

Figure 15: Mean migration speed of NR6 cells in scaffolds with a constant microstructure (pore size 96 µm) but varying strut modulus E_s[10].

The effects of mechanical constraint and cyclic tensile strain on the chondrogenic differentiation of Mesenchymal Stem Cells (MSCs) in a scaffold were investigated in McMahon et al.[12] using a custom-designed 5-station uniaxial stretching bioreactor that could apply cyclic tensile loading to scaffolds. They investigated the effect of constraining the scaffold, applying harmonic stretching (ε=10%, f=1Hz) and chondrogenic growth factors on the chondrogenic differentiation of MSCs inside CG scaffolds. Results demonstrate that cyclic stretching under the specified parameters resulted in a significant increase in GAG synthesis relative to the constrained condition, which indicates that mechanical stimulation influenced the differentiation process.

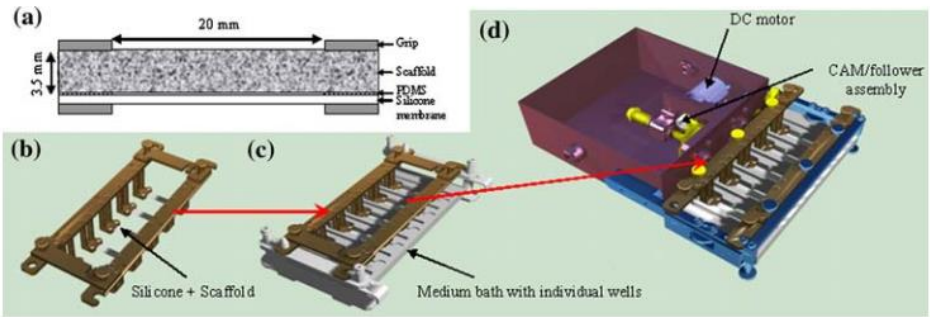

Figure 16: (a) schematic of an experimental set-up for scaffold tensile stretching experiments. The scaffold is attached to a silicone membrane with liquid PDMS, (b) clamping frame containing collagen-GAG scaffolds, (c) clamping frame slotted into static culture frame with individual wells in the medium bath for each construct, and (d) 5-station uniaxial stretching rig, fabricated for use in the dynamic tensile loading experiments[12].

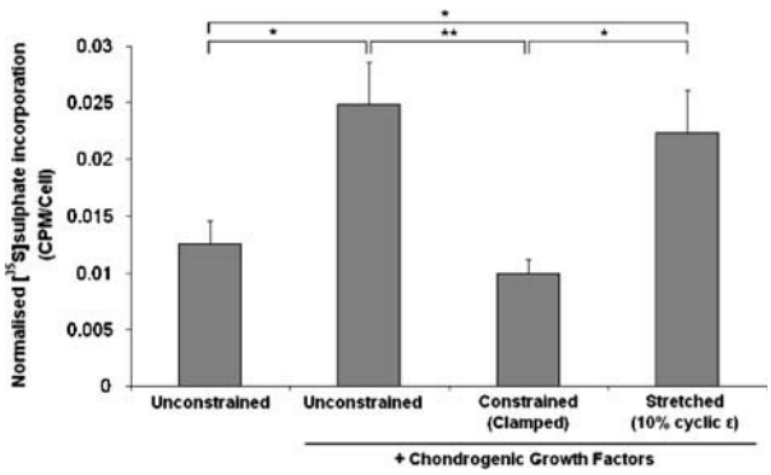

Figure 17: The effect of mechanical constraint and cyclic loading on the chondrogenic differentiation of MSCs in a collagen GAG scaffold[12].

Byrne et al. examined how marrow stromal cell (MSCs) gene expression is affected by pore size, mechanical constraint, and uniaxial cyclic strain when grown inside a porous CG scaffold[13]. They measured RNA amount for type I collagen (Col I), an early marker of osteogenesis, and osteocalcin (OCN), a late marker associated with mineralization, as well as for two additional bone-associated markers, osteopontin (OPN) and bone sialoprotein (BSP), in MSCs cultured in two experiments. In the first experiment, they examined how the scaffold pore size (96, 110 and 151 μm) regulates MSC osteodifferentiation. Results show that pore size had significant effects on the RNA expression of Col I, OPN and OCN, with larger pore environments tending to accelerate induction or increase levels of these RNAs.

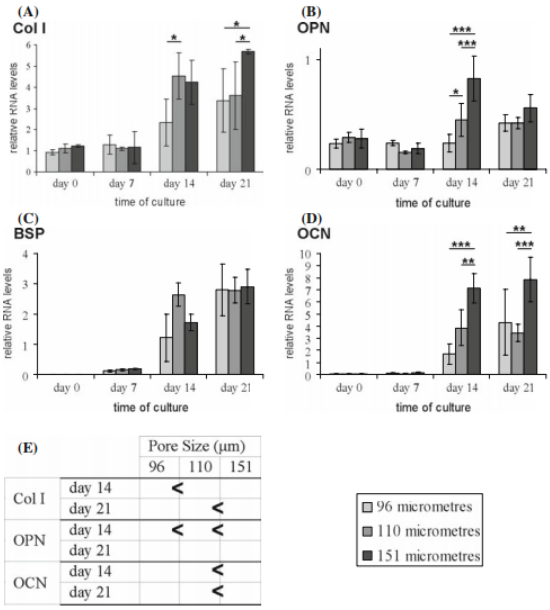

Figure 18: Relative levels of bone associated RNAs from MSC-seeded CG scaffold variants of 96, 110 or 150 μm average pore size. Part E: Summary of significant differences in gene expression between scaffolds of different pore size at each time point, where scaffold(s) to the left of the symbol ''<'' have a lower level of expression than scaffold(s) to the right[13].

In the second experiment, they applied mechanical constraint and uniaxial cyclic strain to MSC-seeded scaffolds in osteogenic medium. Rectangular pieces of scaffold (96 μm pore size) were clamped in mechanical rigs. In the 5th day of culture, they applied, by a stretching device, 5% cyclic strain at 1 Hz for 4 h. Results suggest that mechanical conditions (clamping, straining) had significant effects on gene expression. Specifically, RNA levels of OPN, BSP and OCN were reduced when cells were grown in clamped scaffolds relative to unconstrained scaffolds. In addition, there was a small but significant increase in OPN RNA in cells grown in clamped scaffolds under stretching. Altogether, data suggest that a freely-contracting CG scaffold provides an environment more conducive to osteogenesis.

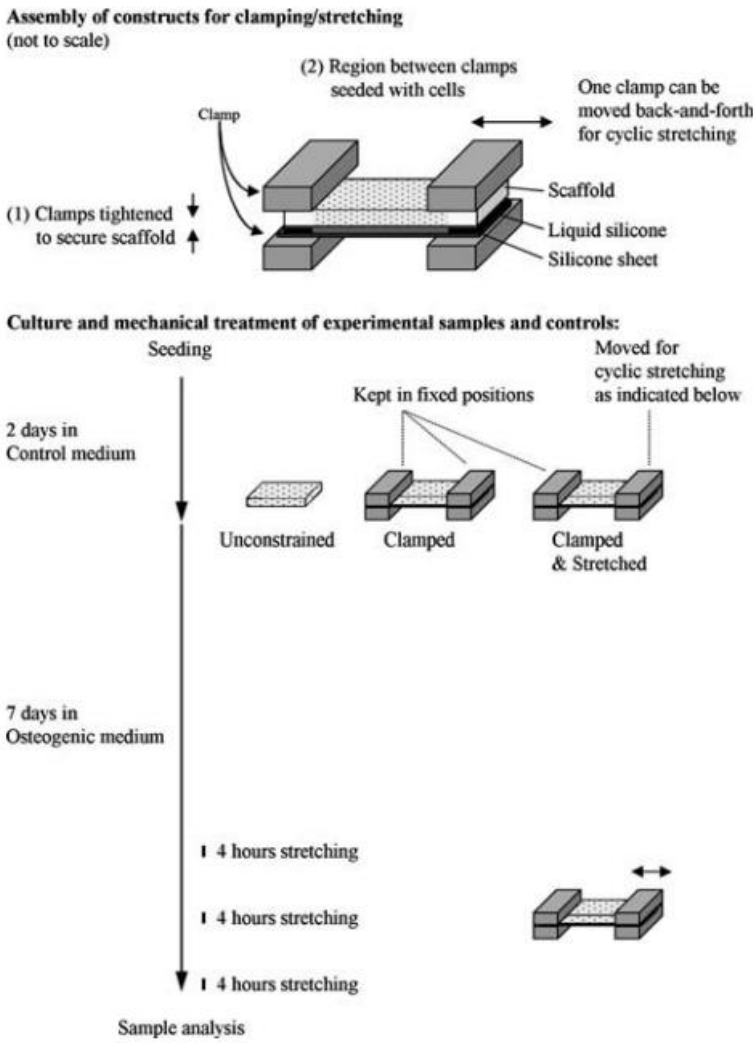

Figure 19: Schematic illustrating set-up of seeded scaffolds in stretching rig[13].

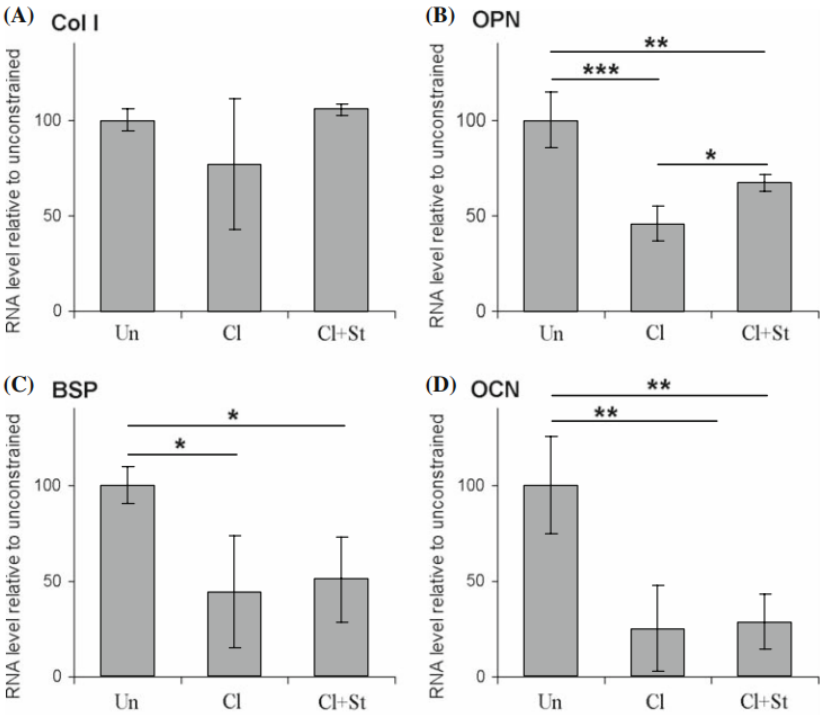

Figure 20: Effects of one-dimensional clamping and 5% uniaxial cyclic strain (1 Hz) on levels of bone-associated RNAs from MSC-seeded CG scaffold constructs incubated for 7 days in the presence of osteogenic factors; constructs were unconstrained (Un), clamped (Cl), or clamped and stretched (Cl + St)[13].

2.4 PCS: Overview and Applications

Porous collagen-based scaffolds (PCS) are biomaterials with extensive clinical applications in regenerative medicine. Grafts based on Porous Collagen Glycosaminoglycan (CG) scaffolds, originally referred to as ''artificial skin''[14–17], are utilized clinically to induce skin regeneration. Similarly, porous collagen scaffolds are utilized clinically to induce regeneration in severely injured (transected) peripheral nerves[18]. Ongoing research efforts focus on developing novel PCS-based grafts that can induce regeneration in a wider variety of injured organs including cartilage[19], tendon[20] and the spinal cord[21]. PCS are also utilized in tissue engineering research. For example, bone tissue engineering research has focused on maximize osteoblast activity by modifying the scaffold composition by varying the amounts of collagen and glycosaminoglycan (GAG)[22]. Porous collagen scaffolds can also support vascularization *in vitro* and *in vivo* in different species (rat and mouse)[23].

Chapter 3: Research methodology

3.1 PCS Fabrication

Porous collagen GAG scaffolds were fabricated by lyophilizing collagen-glycosaminoglycan (CG) suspension using a previously-described method that provides scaffolds of homogeneous pore structure. [24] Type I collagen was dispersed in 50 mM acetic acid solution, poured on stainless steel molds and freeze-dried (final freezing temperature -40°C). Scaffold sheets were cross-linked by dehydrothermal treatment (105°C, 24h), a process that slightly increases scaffold stiffness.

3.2 Fabrication of Microstructures in PCS

Using a femtosecond (fs) laser Yb: KGW (Pharos-SP, Light Conversion) different microstructures were fabricated in PCS. The laser wavelength was 1026nm, the pulse width was 170 fs and pulse frequencies of 1 kHz and 5 kHz were used. An 10x objective lens (Mitutoyo Plan Apo Infinity Corrected Long WD Objective, 0.28NA, f = 200 mm) was used.

Collagen (C) or collagen-glycosaminoglycan (CG) sheets were placed to a glass microscope slide (Thermo Scientific SuperFrost Microscope Slides, Ground 90°) and fastened to the sides with double side tape (Melca Double Sided Tape).

By using ''CSV (comma delimited)'' excel files and g-code, the desirable patterns were fabricated in a 6x4 mm scaffold. Four different patterns were used: parallel horizontal lines (39 lines total, 60 μm width with 70 μm gap between them and 300μm depth of cut), concentric circles (14 circles total, 60 μm width with 70 μm gap between them and 300μm depth of cut), hole (1.5 mm diameter) in the center of the scaffold and a plain ''control'' scaffold. In all scaffolds 2 small holes (600μm or 750μm diameters) in the right and the left sides were fabricated in order to attached later in plastic bases.

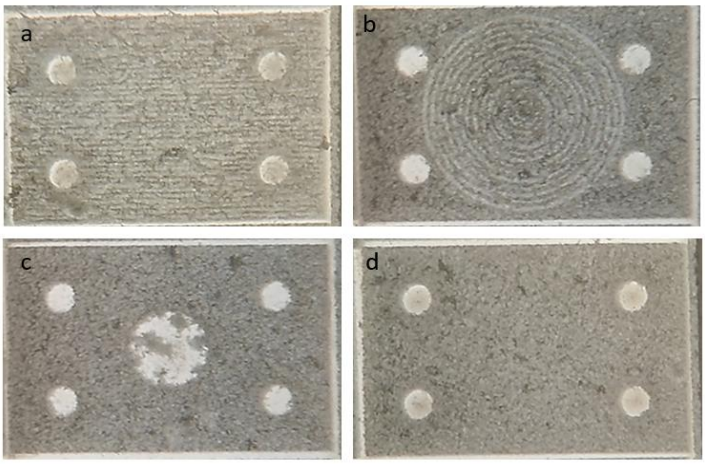

Figure 21: a) Parallel horizontal lines, b) Concentric circles, c) Hole in the center of the scaffold and d) Plain ''control'' scaffold.

3.3 Embryonic Neural Stem Cell Culture

The following protocol is adapted from the M.Sc. thesis of F. Bampoula. Primary E13.5 NSCs were isolated from C57BL/6 embryos at gestational day 13.5 as described previously[21]. Cortical hemispheres were dissected and mechanically dissociated into full NSC medium. $25*10^4$ NSCs were cultured in T25 flasks (Nunc™ EasYFlask™ Cell Culture Flasks, 156367, Thermo-Fisher) in 5ml of full NSC medium consisting of DMEM/F-12 Ham Nutrient Mixture (Sigma D6421), B27 Supplement minus vitamin A (Thermo 12587010), 0.6% D-glucose (Sigma G8769), 100 µg/ml primocin (Invivogen ant-pm-1), 20 ng/ml EGF (R&D 236-EG-200), and 20 ng/ml FGF-2 (R&D, 233-FB-025). NSCs were subcultured when the neurosphere diameter reached approximately 100 µm and the neurosphere center remained bright (after 4-5 days of culture). Neurospheres were dissociated into a single-cell suspension after a 6 min incubation (37^oC) with accutase (Sigma A6964). Cells were ready for experiments at 4th passage after isolation.

In 3D cultures, E13.5 NSCs were seeded in porous collagen scaffolds as single-cell suspension. A drop of $2*10^4$ cells in 20 µl full NSC medium was placed at the top of the upside down scaffold in a 12-well plate. After 15 min of incubation at 37^oC the base with the scaffold turns over and 500µl NSC full medium were added per well.

After cell seeding in full NSC medium, cells were cultured in order to proliferate and grow for two days *in vitro*. At 2DIV, the medium was switched into neural differentiation medium consisting of full NSC medium without EGF and FGF. Cells were cultured in differentiation medium for five more days (until 7DIV).

3.4 NIH-3T3 Culture

In an amount of $25*10^4$ NIH-3T3 cells were cultured in T25 flasks (Nunc 156367) into 5ml of culture medium consisting of high glucose DMEM (Thermo 41966029), 10% FBS (Thermo 10270-106) and 1% Penicillin/Streptomycin (Thermo 15140-122).

In 3D cultures, NIH-3T3 were seeded in porous collagen scaffolds as single-cell suspension. A drop of $2*10^4$ cells in 20µl medium was placed at the top of the upside down scaffold in a 12-well plate. After 15 min of incubation at 37^oC the base with the scaffold turn over and 500µl medium were added per well. After cell seeding, cells were cultured in order to proliferate and grow for a maximum of 8 days in vitro (8DIV).

3.5 Immunocytochemistry

Cells were fixed with 4% paraformaldehyde (20min) at the desirable stage of culture and then stained using primary antibodies for markers of interest.

3.5.1 Tubulin β3

Tubulin beta 3 (TUBB3) was used as a marker of neurons using an anti-tubb3 antibody (1:1000, MAB1637, Millipore) and anti-mouse Alexa488-conjugated secondary antibody (1:1000, A11029, Thermo). Tuj1 staining is cytoplasmic (Figure 22).

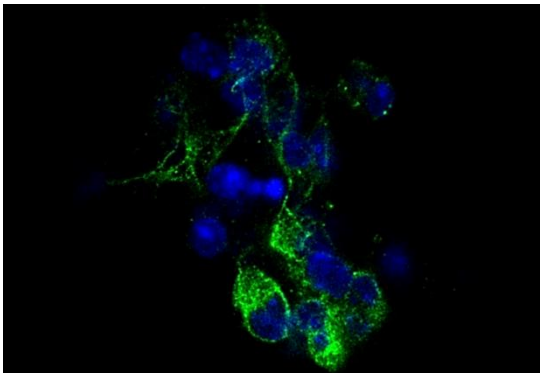

Figure 22: Tuj1 (green) and Hoechst (blue) staining.

3.5.2 GFAP

GFAP was used as a marker of astrocytes using an anti-GFAP primary antibody (1:1000, Millipore ab5541) and anti-chicken Alexa546-conjugated secondary antibody (1:1000, A11040, Life Technologies). GFAP staining is cytoplasmic (Figure 23).

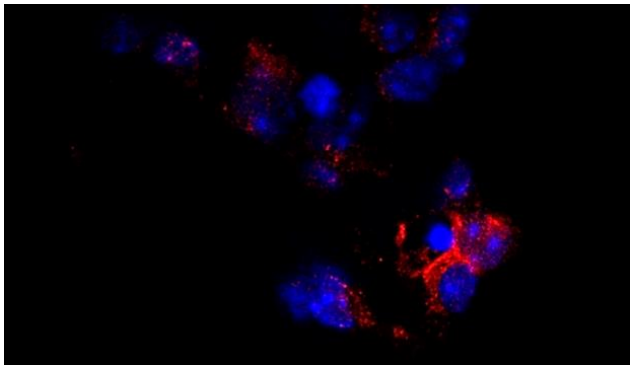

Figure 23: GFAP (red) and Hoechst (blue) staining.

3.5.3 α-SMA

α-SMA (α-Smooth muscle actin) was used as the marker of myofibroblasts using a mouse anti-aSMA antibody (Sigma A5228, 1:200) and an anti-mouse Alexa488-conjugated secondary antibody (1:1000, A11029, Thermo). α-SMA staining is cytoplasmic (Figure 24).

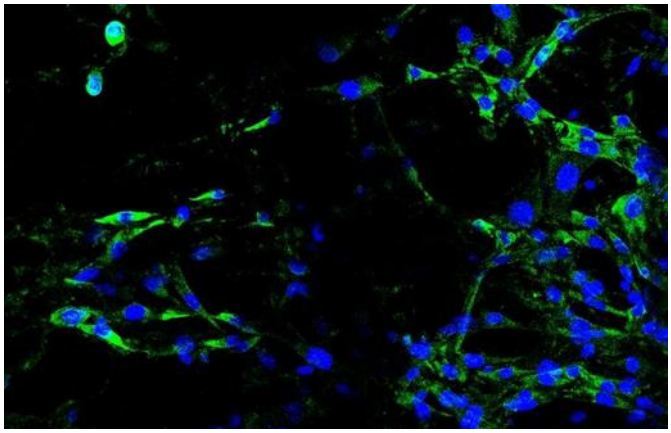

Figure 24: α-SMA (green) and Hoechst (blue) staining.

3.5.4 Phalloidin

Phalloidin 633 was used to counter stain actin filaments (also known as F-actin). Phalloidin staining is cytoplasmic (Figure 25).

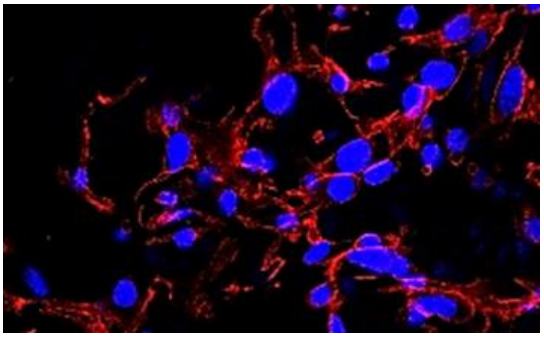

Figure 25: Phalloidin (red) and Hoechst (blue) staining.

3.6 Image Acquisition

Cells-seeded scaffolds were placed on a glass-bottom plastic plate within a drop of PBS. Images were acquired using a Leica TCS SP8 inverted confocal microscope using a 40x water-immersion objective lens or a 10x dry objective lens. By visualizing Hoechst33342-stained cell nuclei using the microscope eyepiece, z-stacks were acquired in about 5 different positions per scaffold. Each position was selected based on Hoechst staining, preferring scaffold sites that contain many cells. The ''Tilescan'' tool of LASx microscope software was used to capture the whole scaffold and "Mark and Find" tool to optimize the stack at each position in order to image as many cells as possible.

Also, a fluorescent microscope was used to examine cell behavior. Cells-seeded scaffolds were maintained in the 12-well plate throughout the imaging process. Images were acquired using 4x and 10x objective lenses. By visualizing CalceinAM, which stains alive cells, different positions per scaffold were acquired.

3.7 Quantification

3.7.1 Cell Counting

All acquired images were processed using the "Cell Counter" Tool of the ImageJ-Fiji software. Selecting "Show All", all counters were visible in all stacks. Firstly, nuclei were marked in all stacks in order to count the total number of cells based on Hoechst33342 staining. Then, in composite display mode with the other channels, antibody staining was marked with a different color of cell counter.

A specific color-rule was utilized for each staining, same in all experiments. Hoechst33342 nucleic acid stain was visualized with blue. Tuj1 staining for neurons was visualized with green and GFAP staining for astrocytes was visualized with red. If around the nucleus, the cell's cytoplasm was green then this cell counted as a neuron. Otherwise, if

around the nucleus, the cell's cytoplasm was red then this cell counted as an astrocyte. In the figure below (Figure 26) a neurosphere is represented. In white circle a neuron is marked and in yellow circles the astrocytes.

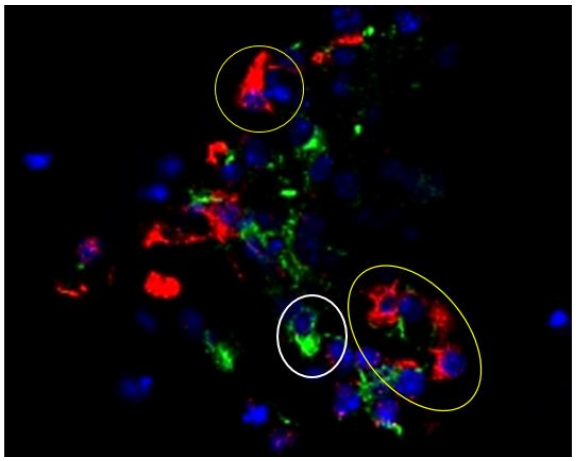

Figure 26: A neuron is marked inside a white circle. Astrocytes are marked inside yellow circles. Tuj1 (green), GFAP (red) and Hoechst (blue) staining.

3.7.2 Statistical Analysis

Results were organized and processed in Excel files. For each experiment, the mean value of each metric of interest (e.g. cell fraction) was calculated as the mean of technical replicates. In NSC differentiation experiments the means of $TUJ1^+$ or $GFAP^+$ cell fractions (four different conditions) were compared using one-way ANOVA analysis using MATLAB built-in functions anova1 and multcompare. In all bar plots, results are presented as mean±s.e.m.

Chapter 4: Research findings / results

4.1 NIH-3T3 Growth and Contraction Inside PCS

In order to examine fibroblast growth and proliferation inside PCS, fibroblasts were seeded and grown inside plain PCS or PCS that contained two different kinds of patterns (concentric circles, a scaffold with a hole in the center). For each scaffold type, the experiment was performed one time. A drop of $2*10^4$ cells in 20μl medium was placed on top and across the length of the scaffold. Images in different days of culture were taken. CalceinAM was used for staining the living cells. Images were acquired using a fluorescent microscope.

Figure 27 shows a microfabricated scaffold with concentric circles. On the 4th day of culture (4DIV) live cells were evenly distributed. This confirms that the cells have been inserted evenly along the entire length of the scaffold. In Figure 27b the cells' axes appear to be parallel to the circles. Also, according to Figure 27b and Figure 28b, the circle structure appears to slightly guide the direction of the cells instead of the control scaffold. Furthermore, one of 4 side holes was broken (Figure 28). Fibroblast are known to exerts significant forces. After 7 days (7DIV) the concentric circles were deformed due to forces exerted by fibroblasts (Figure 29). NIH3T3 had multiplied and grown a lot. At 8DIV, the scaffold was fixed, immunostained for α-SMA and counterstained with Phalloidin. Figure 30 shows that fibroblasts exert great forces due to the fact that the phalloidin stains F-actin filaments which are part of the contractile apparatus in muscle. Also Figure 31 shows that cells stained with phalloidin appears to be guided through the outline of the circles (pointed with white arrows).

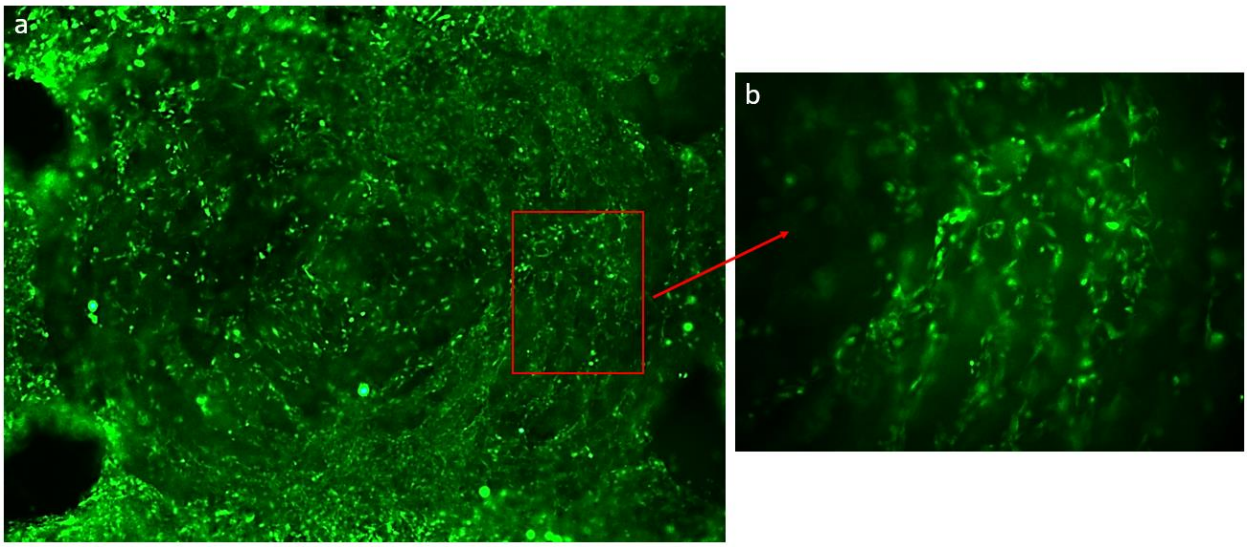

Figure 27: NIH-3T3 seeded in PCS patterned with concentric circles cultured at *4DIV. Image from fluorescent microscope stained with CalceinAM (green).*

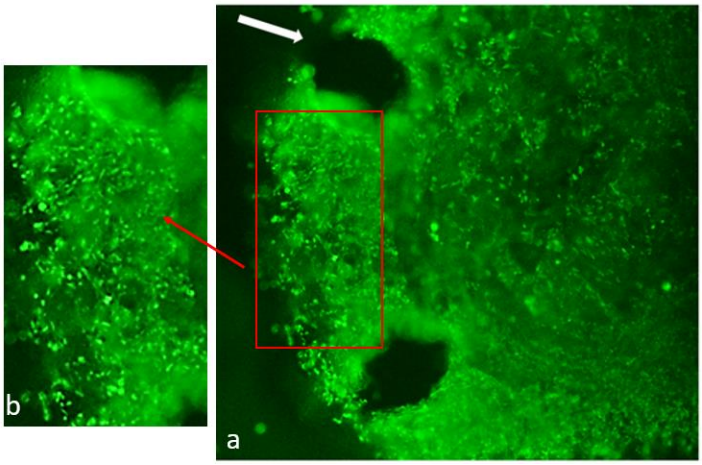

Figure 28: NIH-3T3 seeded in PCS patterned with concentric circles cultured at *4DIV. Image from fluorescent microscope stained with CalceinAM (green). One of the four side holes was broken.*

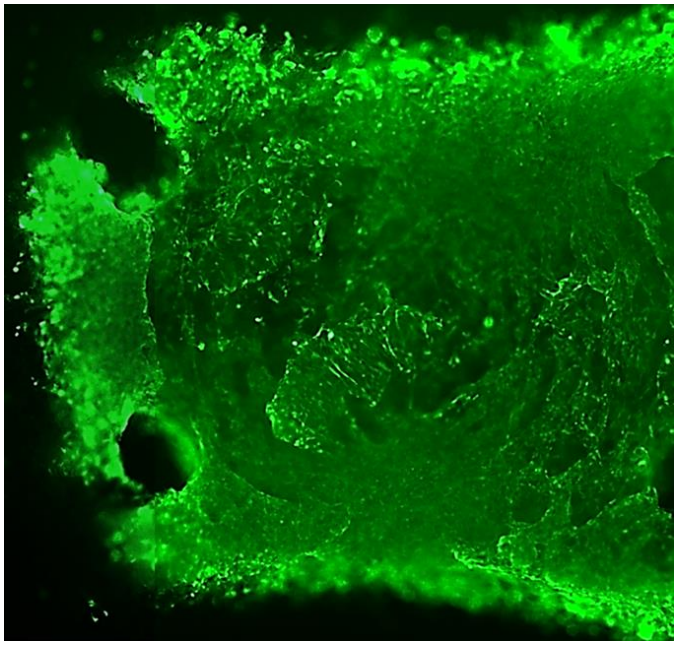

Figure 29: NIH-3T3 seeded in PCS patterned with concentric circles cultured at *7DIV. Image from fluorescent microscope stained with CalceinAM (green). The concentric circles were deformed.*

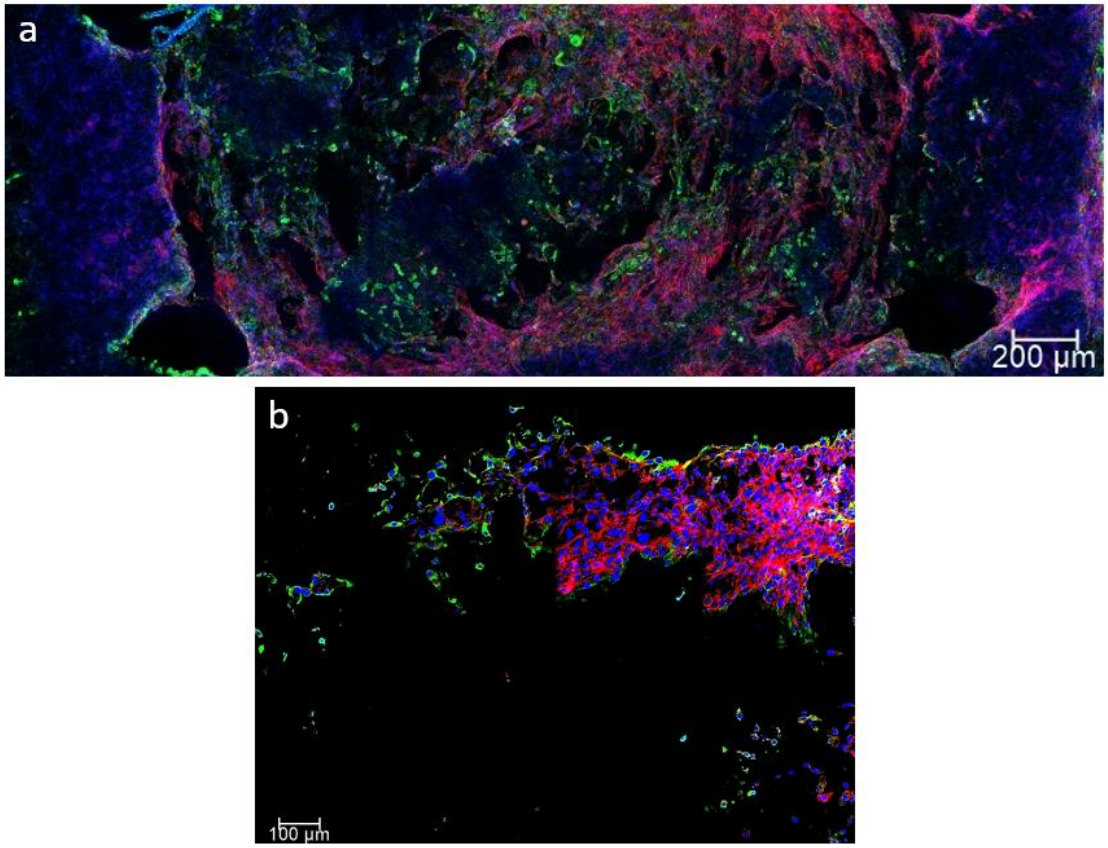

Figure 30: NIH-3T3 seeded in PCS patterned with concentric circles cultured at *8DIV. Images from confocal microscopy. a) the whole scaffold in maximum projection of all stacks and b) a part of it. Staining with α-SMA (green), Phalloidin (red) and Hoechst (blue).*

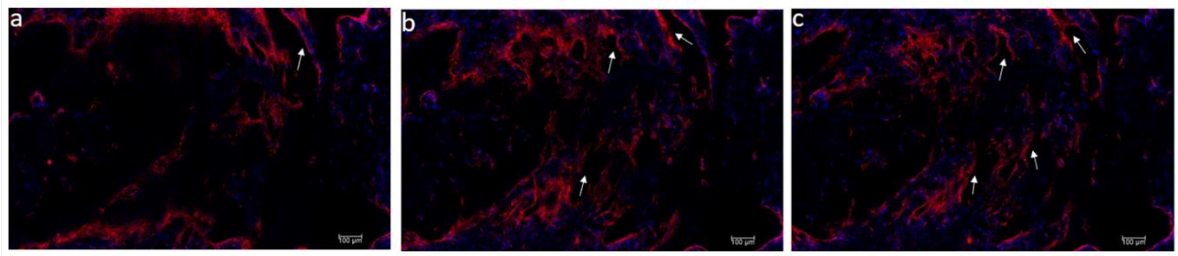

Figure 31: NIH-3T3 seeded in PCS patterned with concentric circles cultured at *8DIV. Images from confocal microscopy. Different stacks inside the scaffold. White arrows point to the areas where cells are guided through the outline of the circles. Staining with α-SMA (green), Phalloidin (red) and Hoechst (blue).*

Another experiment was to seed fibroblasts on a scaffold with a hole in the center and in a ''plain'' control scaffold. After 2DIV the living cells were evenly spread (Figure 32 and Figure 33). The middle hole had acquired an elliptical shape due to the cells' forces.

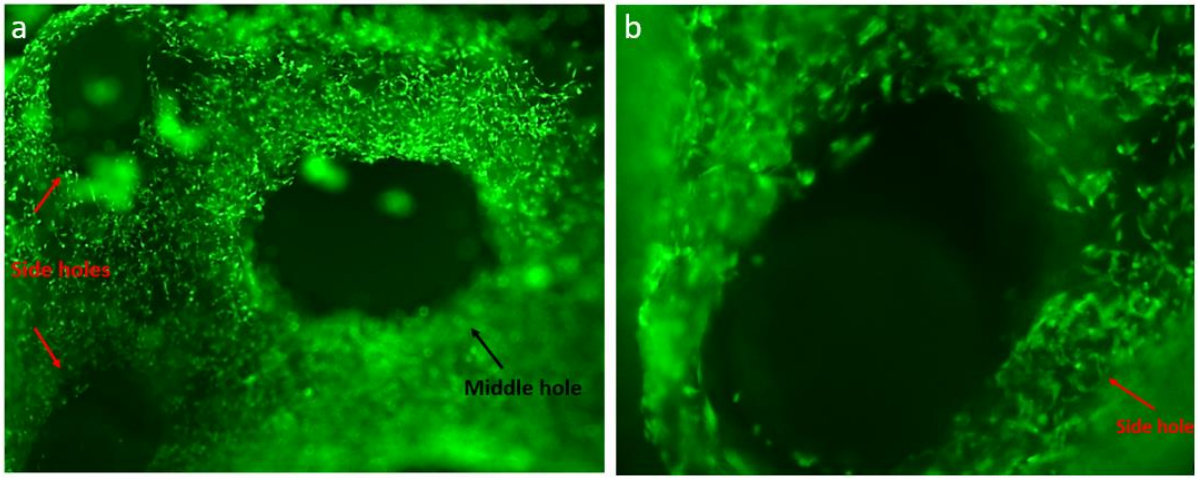

Figure 32: NIH-3T3 seeded in PCS patterned with a hole in the middle cultured at *2DIV. Images from fluorescent microscope stained with CalceinAM (green).*

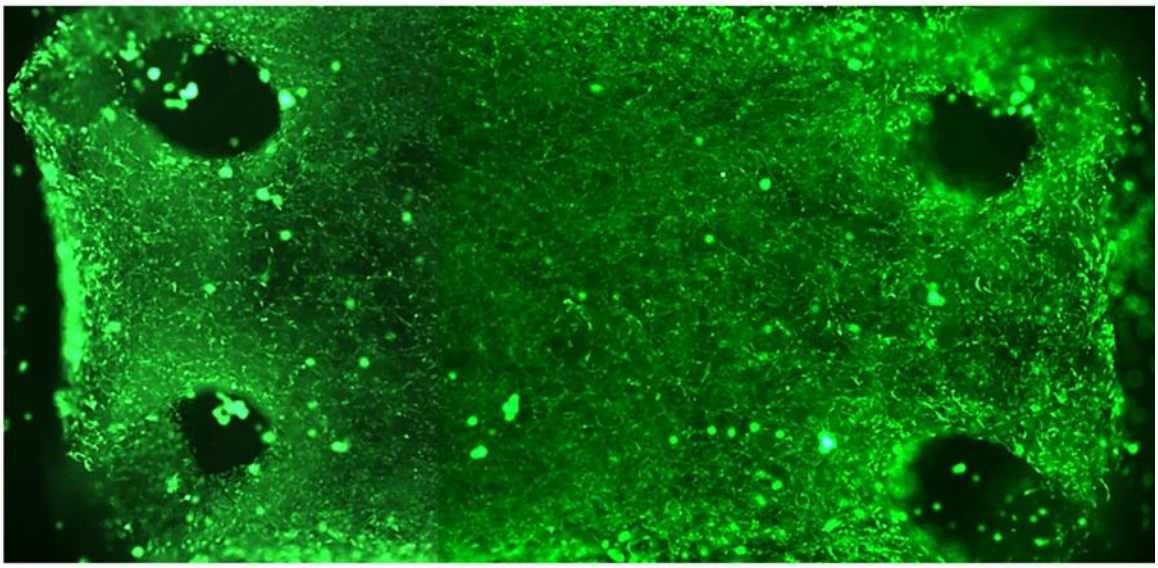

Figure 33: NIH-3T3 seeded in a ''plain'' control PCS cultured at *2DIV. Image from fluorescent microscope stained with CalceinAM (green).*

4.2 NSC Growth and Differentiation Inside PCS

In order to quantify the effect of NSC-matrix interactions on NSC differentiation, NSC were seeded in four kinds of PCS: plain PCS, PCS with parallel horizontal lines, PCS with concentric circles, and PCS with a hole in the center. For each type of PCS, the experiment was performed for a minimum of 3 times. A drop of $2*10^4$ cells in 20 μl medium was placed on top and across the length of the scaffold. Images in different days of culture were taken. At 7DIV, scaffolds were fixed and stained for markers of differentiated neural cells: Tuj1 (neuronal marker) and GFAP (astrocytes marker). As shown in Figure 34, NSCs grew in clusters. The fraction of cells that stain for Tuj1 and GFAP were quantified manually.

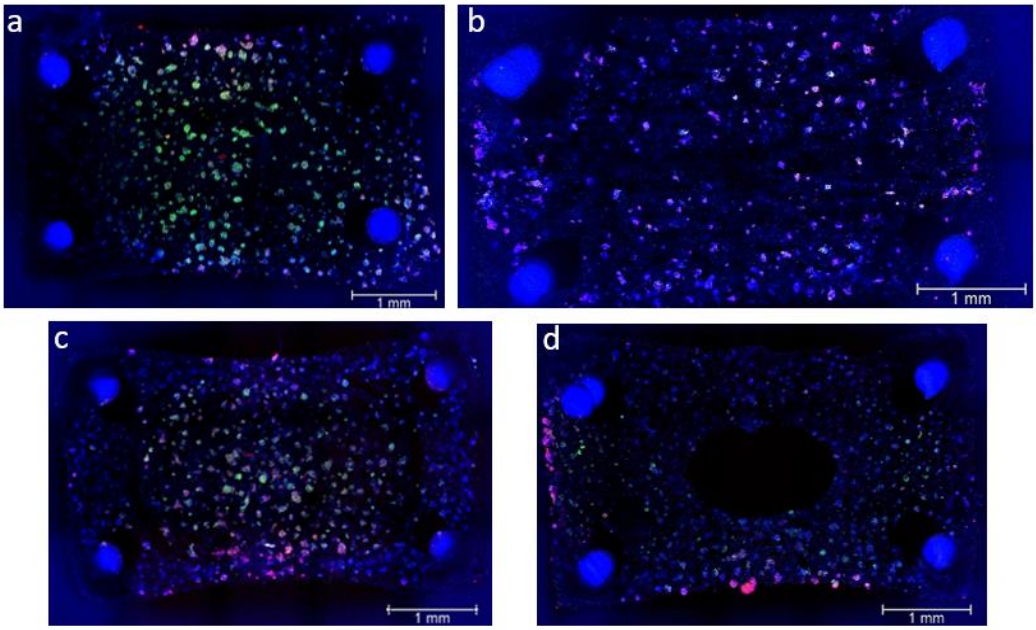

Figure 34: Growth of NSC inside PCS cultured for 7DIV in a) a plain ''control'' scaffold b) a PCS that contains parallel horizontal lines, c) a PCS that contains concentric circles, d) a PCS that contains a hole in the center of the scaffold. Staining with Tuj1 (green), GFAP (red), Hoechst (blue). Maximum projection of all stacks.

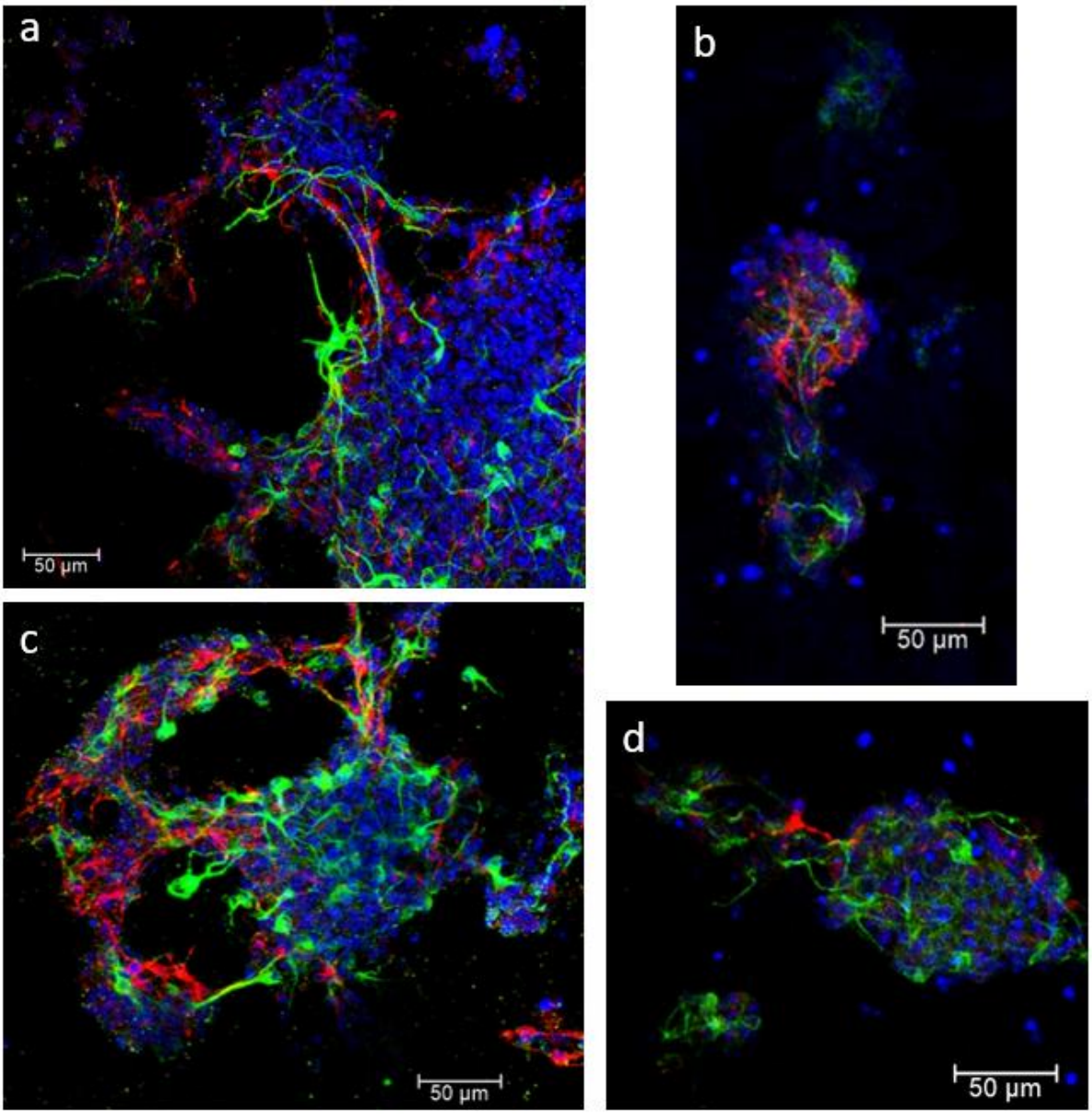

Figure 35: Growth of NSC inside a ''plain'' control PCS at 7DIV. Staining with Tuj1 (green), GFAP (red), Hoechst (blue). Maximum projection of all confocal z-stacks.

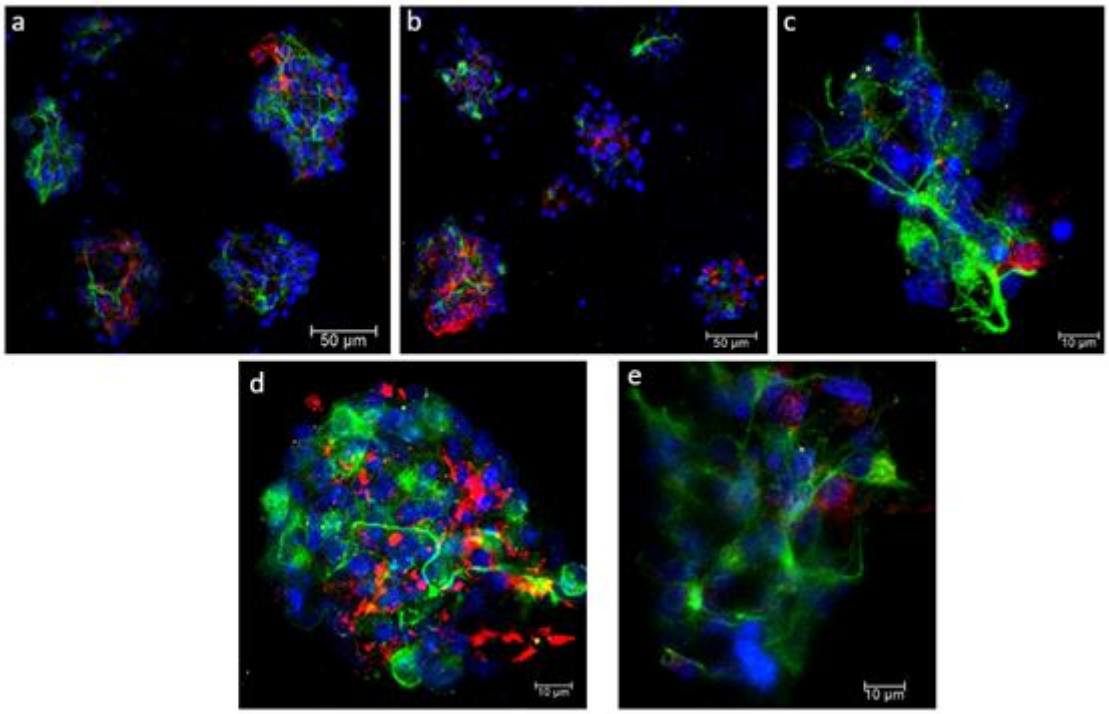

Figure 36: Growth of NSCs inside PCS that contain parallel horizontal lines at 7DIV. Staining with Tuj1 (green), GFAP (red), Hoechst (blue). Maximum projection of all stacks.

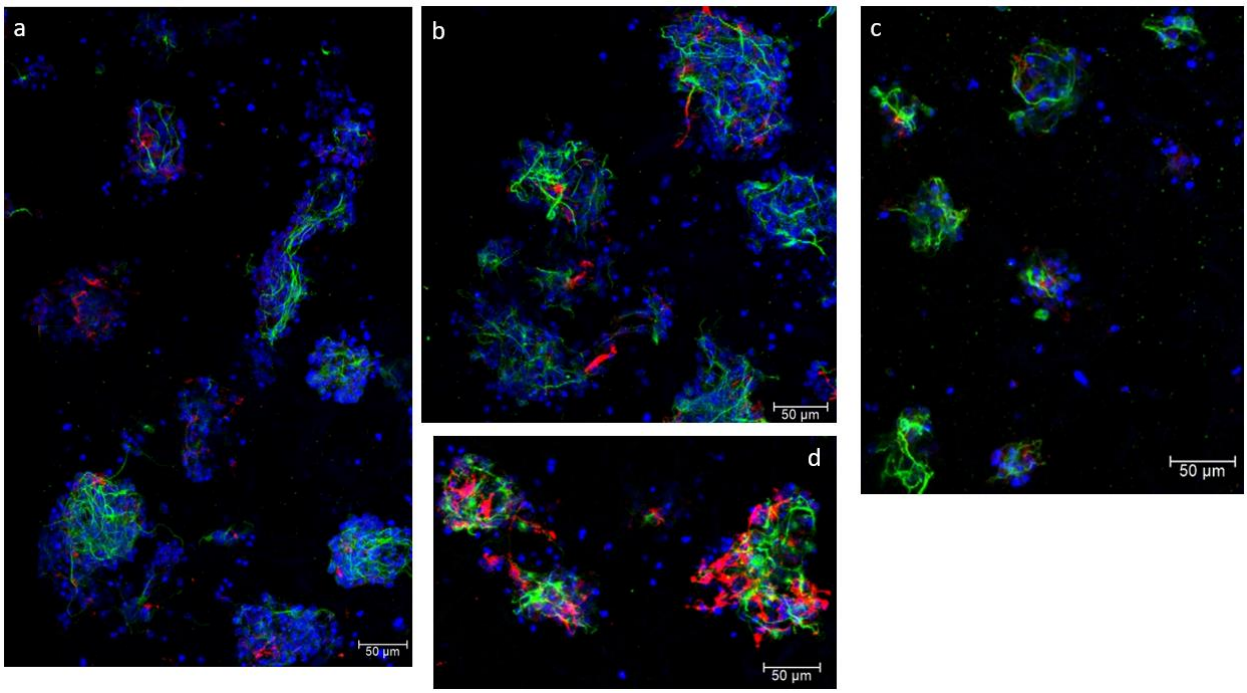

Figure 37: Growth of NSC inside PCS that contain concentric circles at 7DIV. Staining with Tuj1 (green), GFAP (red), Hoechst (blue). Maximum projection of all stacks.

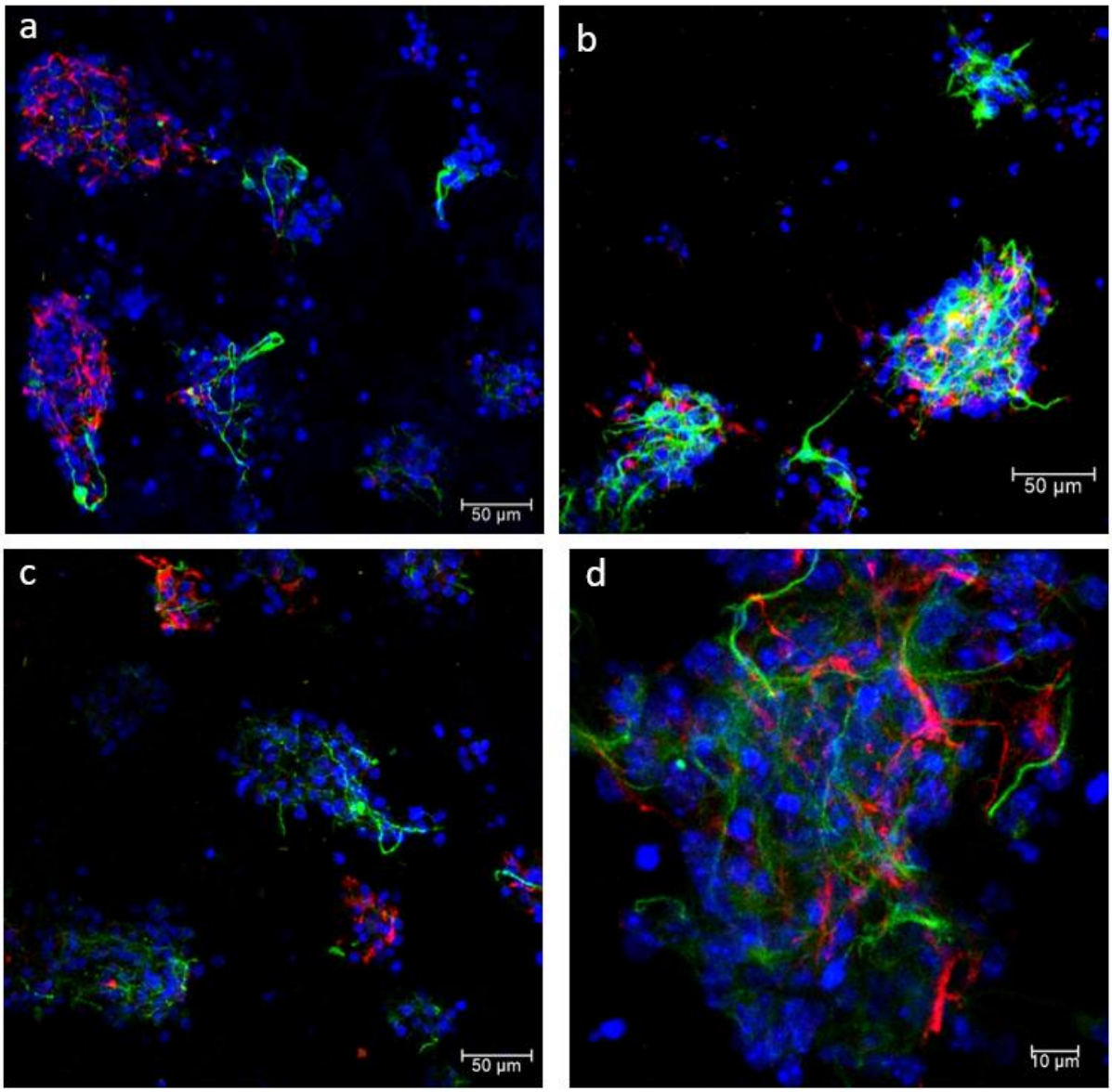

Figure 38: Growth of NSC inside PCS that contain a hole in the middle at 7DIV. Staining with Tuj1 (green), GFAP (red), Hoechst (blue). Maximum projection of all stacks.

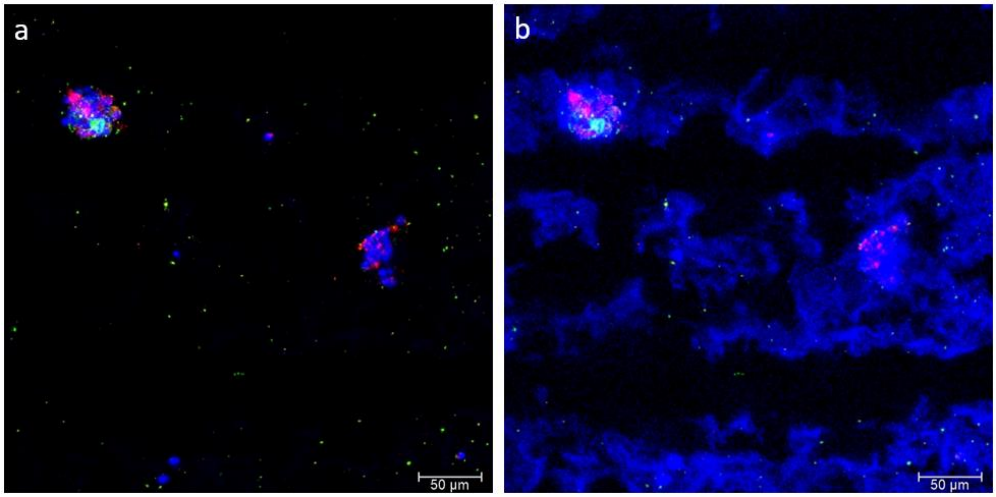

Figure 39: Growth of NSCs inside PCS that contain parallel horizontal lines cultured at7DIV. b) The same image, processed in order to visualize clearly the parallel horizontal lines. Staining with Tuj1 (green), GFAP (red), Hoechst (blue). Maximum projection of all stacks.

Graph 1 shows the fraction of TUJ1$^+$ cells (differentiated to neurons) for the four different patterns is given. Results show that the fraction of TUJ1$^+$ cells (mean ± s.e.m.) in the control plain scaffold is 19.5±1.4 %, in the PCS that contains lines is 21.5±3.7 %, in the PCS that contains circles is 12.7±1.3 %, and in the PCS that contains a hole is 19.2±7.1 %.

Graph 2 shows the fraction of GFAP$^+$ cells (differentiated to astrocytes) for the 4 different patterns. Results show that the fraction of GFAP$^+$ cells (mean ± s.e.m.) for the control "plain" PCS is 18.0±2.5 %, in the PCS that contains lines is 20.3±5.9 %, in the PCS that contains circles is 9.5±1.3 %, and in the PCS that contains a hole is 16.4±4.7 %. For the pattern with the hole in the middle, the variation (described by the s.e.m.) appears to be higher than the other patterns. One possible reason is that in different areas in the scaffolds there are different strains, and this can cause variability in the results. In contrast, in control plain scaffolds, PCS that contain lines and PCS that contain circles, have similar mean values. Due to the fact that in the control scaffold the strain field is similar in the whole scaffold, the strain in different regions appears to be about the same. This shows that the pattern with the lines does not affect the stain field or the cells. In the scaffold with the hole in the middle, there is a region (above and under the hole) with high strain but in the other regions the strains are similar to the control scaffold. From the Graphs below we can suggest that the pattern with the concentric circles can affect the differentiation of the NSCs. A possible way for this to happen is that the concentric circles changed the strain that the cells feel.

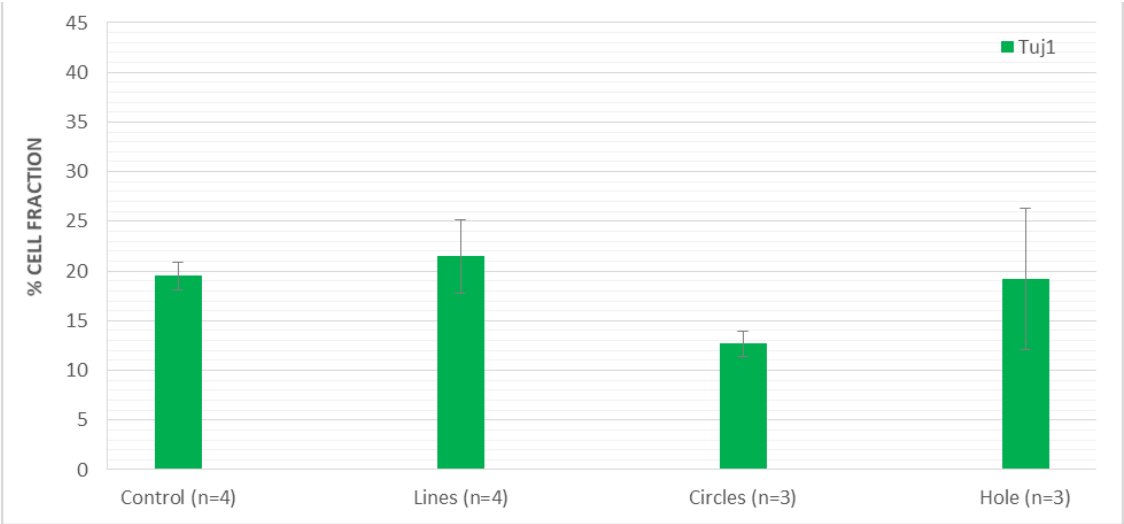

Graph 1: Fraction of TUJ1⁺ cells when NSCs are grown in four different kinds of scaffolds at 7DIV.

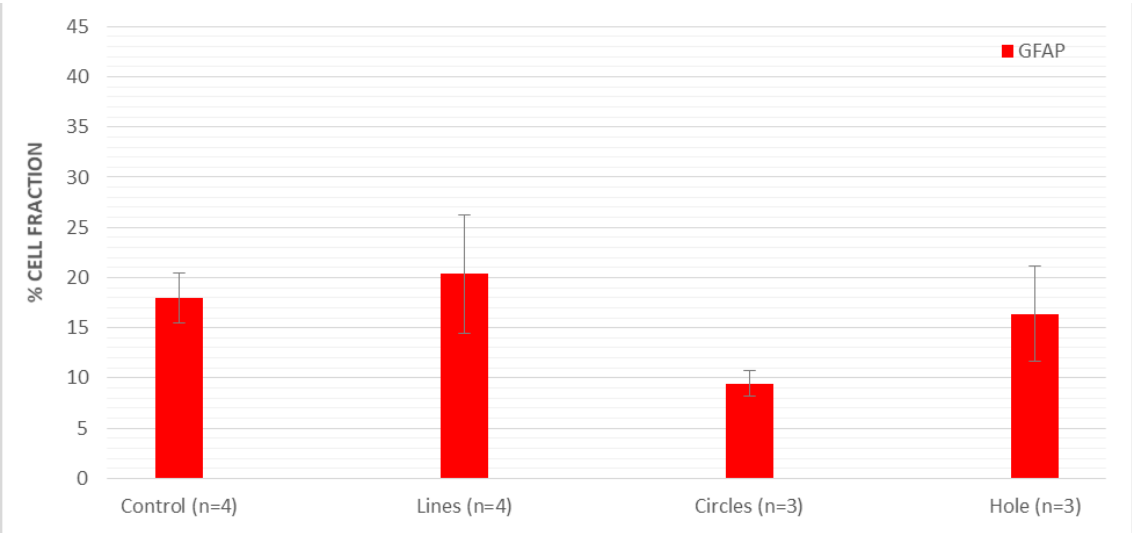

Graph 2: Fraction of GFAP⁺ cells when NSCs are grown in four different kinds of scaffolds at 7DIV.

Statistical analysis showed that the fraction of TUJ1⁺ cells do not differ significantly among the 4 groups. For the TUJ1⁺ P1-way anova was 0.4546 and for the GFAP⁺ P1-way anova was 0.37821. Although the data shows an effect for the group with the concentric circles, statistics shows no difference because of the small number of n (n=3-4 for each group).

Chapter 5: Discussion and analysis of findings

Experiments on the growth of NIH-3T3 cells inside PCS suggest that fibroblasts exert great forces as they significantly deform the scaffold. It appears that the pattern of concentric circles slightly affects fibroblast formation as their axes appeared to be parallel with the circles.

Experiments on NSC differentiation inside PCS show that in control “plain” scaffolds the strain field is mainly axial and generally evenly. In PCS that contain lines the strain field is also axial and evenly. This observation could explain why there are no differences in NSC differentiation towards the neuronal and astrocyte fates. In PCS that contain a hole in their middle, large axial strains are expected in the regions exactly above and under the hole. In PCS that contain microfabricated circles, it is possible that in the proximity of the circular patterns there is a change in the strain field and that’s why there is a difference in the results.

Furthermore, another possible experiment is to seed NSCs in scaffolds that are not stabilized (free in culture). Such experiments in smaller ‘’plain’’ scaffolds have shown a 10% differentiation. Here, our results showed approximately 19% of differentiation.

References

1. Stabley, D. R., Jurchenko, C., Marshall, S. S. & Salaita, K. S. Visualizing mechanical tension across membrane receptors with a fluorescent sensor. *Nat. Methods* **9**, 64–67 (2012).

2. Dembo, M. & Wang, Y. L. Stresses at the cell-to-substrate interface during locomotion of fibroblasts. *Biophys. J.* **76**, 2307–2316 (1999).

3. Tan, J. L. *et al.* Cells lying on a bed of microneedles: An approach to isolate mechanical force. *Proc. Natl. Acad. Sci. U. S. A.* **100**, 1484–1489 (2003).

4. Legant, W. R. *et al.* Measurement of mechanical tractions exerted by cells in three-dimensional matrices. *Nat. Methods* **7**, 969–971 (2010).

5. Gjorevski, N. & Nelson, C. M. Mapping of mechanical strains and stresses around quiescent engineered three-dimensional epithelial tissues. *Biophys. J.* **103**, 152–162 (2012).

6. Notbohm, J. *et al.* Three-dimensional traction force microscopy for studying cellular interactions with biomaterials. *Procedia IUTAM* **4**, 144–150 (2012).

7. Maskarinec, S. A., Franck, C., Tirrell, D. A. & Ravichandran, G. Quantifying cellular traction forces in three dimensions. *Proc. Natl. Acad. Sci. U. S. A.* **106**, 22108–22113 (2009).

8. Herrera, A. *et al.* From macroscopic mechanics to cell-effective stiffness within highly aligned macroporous collagen scaffolds. *Mater. Sci. Eng. C* **103**, 109760 (2019).

9. Corin, K. A. & Gibson, L. J. Cell contraction forces in scaffolds with varying pore size and cell density. *Biomaterials* **31**, 4835–4845 (2010).

10. Harley, B. A. C. *et al.* Microarchitecture of three-dimensional scaffolds influences cell migration behavior via junction interactions. *Biophys. J.* **95**, 4013–4024 (2008).

11. Harley, B. A., Leung, J. H., Silva, E. C. C. M. & Gibson, L. J. Mechanical characterization of collagen-glycosaminoglycan scaffolds. *Acta Biomater.* **3**, 463–474 (2007).

12. McMahon, L. A., Reid, A. J., Campbell, V. A. & Prendergast, P. J. Regulatory effects of mechanical strain on the chondrogenic differentiation of MSCs in a collagen-GAG scaffold: Experimental and computational analysis. *Ann. Biomed. Eng.* **36**, 185–194 (2008).

13. Byrne, E. M. *et al.* Gene expression by marrow stromal cells in a porous collagen-glycosaminoglycan scaffold is affected by pore size and mechanical stimulation. *J. Mater. Sci. Mater. Med.* **19**, 3455–3463 (2008).

14. Yannas, I. V, Lee, E., Orgill, D. P., Skrabut, E. M. & Murphy, G. F. Synthesis and characterization of a model extracellular matrix that induces partial regeneration of adult mammalian skin. *Proc. Natl. Acad. Sci. U. S. A.* **86**, 933–7 (1989).

15. Coughlin, P. Wound Tissue Can Utilize a Polymeric Template to Synthesize a Functional Extension of Skin. **215**, 174–176 (1982).

16. Orgill, D. P. & Yannas, I. V. Design of an artificial skin . IV . Use of island graft to isolate organ regeneration from scar synthesis and other processes leading to skin wound closure. 1–5 (1997).

17. Compton, C. C., Butler, C. E., Yannas, I. V, Warland, G. & Orgill, D. P. Collagen-GAG Matrices Seeded with Autologous Keratinocytes. 908–916 (1998).

18. Soller, E. C., Tzeranis, D. S., Miu, K., So, P. T. C. & Yannas, I. V. Common features of optimal collagen scaffolds that disrupt wound contraction and enhance regeneration both in peripheral nerves and in skin. *Biomaterials* **33**, 4783–4791 (2012).

19. Matsiko, A., Levingstone, T. J., O'Brien, F. J. & Gleeson, J. P. Addition of hyaluronic acid improves cellular infiltration and promotes early-stage chondrogenesis in a collagen-based scaffold for cartilage tissue engineering. *J. Mech. Behav. Biomed. Mater.* **11**, 41–52 (2012).

20. Hortensius, R. A., Ebens, J. H., Dewey, M. J. & Harley, B. A. C. Incorporation of the Amniotic Membrane as an Immunomodulatory Design Element in Collagen Scaffolds for Tendon Repair. *ACS Biomater. Sci. Eng.* **4**, 4367–4377 (2018).

21. Kourgiantaki, A. *et al.* Neural stem cell delivery via porous collagen scaffolds promotes neuronal differentiation and locomotion recovery in spinal cord injury. *npj Regen. Med.* **5**, 1–14 (2020).

22. Tierney, C. M., Jaasma, M. J. & Brien, F. J. O. Osteoblast activity on collagen-GAG scaffolds is affected by collagen and GAG concentrations. (2008) doi:10.1002/jbm.a.32207.

23. Chan, E. C. *et al.* Three dimensional collagen scaffold promotes intrinsic vascularisation for tissue engineering applications. *PLoS One* **11**, 1–15 (2016).

24. O'Brien, F. J., Harley, B. A., Yannas, I. V. & Gibson, L. Influence of freezing rate on pore structure in freeze-dried collagen-GAG scaffolds. *Biomaterials* **25**, 1077–1086 (2004).